Cell Reports

Article

Perturbations in 3D genome organization can promote acquired drug resistance

Graphical abstract

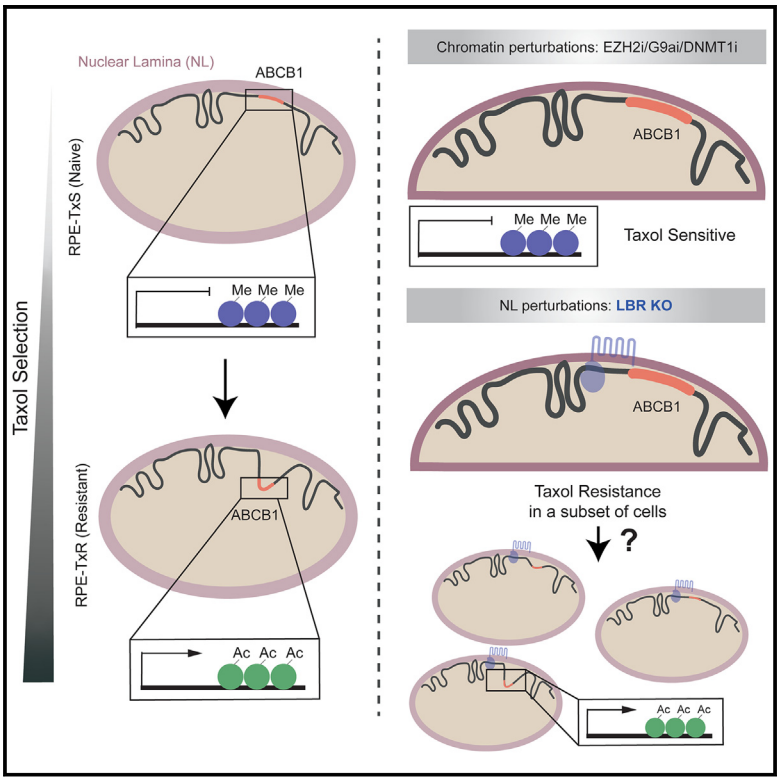

Highlights

- Taxol resistance in RPE cells results from *ABCB1* gene re-activation
- Taxol-resistant cells display altered chromatin marks and NL interactions at the *ABCB1* locus
- Modifying chromatin marks with inhibitors has limited impact on *ABCB1* expression
- Loss of LBR facilitates *ABCB1* derepression upon Taxol exposure

Authors

Anna G. Manjón, Stefano Giustino Manzo, Stefan Prekovic, ..., Elzo de Wit, Bas van Steensel, René H. Medema

Correspondence

b.v.steensel@nki.nl (B.v.S.), r.medema@nki.nl (R.H.M.)

In brief

Manjon et al. demonstrate that Taxol resistance in cells arises from *ABCB1* gene activation, linked to altered histone modifications and 3D genome topology, especially in NL interactions. Inhibition of repressive chromatin modifiers had no impact on *ABCB1* expression, while LBR disruption led to Taxol resistance in a subset of cells.

Manjón et al., 2023, Cell Reports *42*, 113124
October 31, 2023
https://doi.org/10.1016/j.celrep.2023.113124

CellPress

Cell Reports

CellPress
OPEN ACCESS

Article

Perturbations in 3D genome organization can promote acquired drug resistance

Anna G. Manjón,[1,2] Stefano Giustino Manzo,[1,3,5] Stefan Prekovic,[1,4,6] Leon Potgeter,[1,2] Tom van Schaik,[1,3] Ning Qing Liu,[3,7] Koen Flach,[3] Daniel Peric-Hupkes,[1,3] Stacey Joosten,[1,4] Hans Teunissen,[3] Anoek Friskes,[1,2] Mila Ilic,[1,2] Dorine Hintzen,[1,2] Vinícius H. Franceschini-Santos,[1,3] Wilbert Zwart,[1,4] Elzo de Wit,[3] Bas van Steensel,[1,3,*] and René H. Medema[1,2,8,*]

[1]Oncode Institute, The Netherlands Cancer Institute, Plesmanlaan 121, 1066CX Amsterdam, the Netherlands
[2]Division of Cell Biology, The Netherlands Cancer Institute, Plesmanlaan 121, 1066CX Amsterdam, the Netherlands
[3]Division of Gene Regulation, The Netherlands Cancer Institute, Plesmanlaan 121, 1066CX Amsterdam, the Netherlands
[4]Division of Oncogenomics, The Netherlands Cancer Institute, Plesmanlaan 121, 1066CX Amsterdam, the Netherlands
[5]Department of Biosciences, Università degli Studi di Milano, Via Celoria 26, 20133 Milan, Italy
[6]Center for Molecular Medicine, University Medical Center Utrecht and Utrecht University, 3584 CX Utrecht, the Netherlands
[7]Department of Hematology, Erasmus Medical Center (MC) Cancer Institute, Rotterdam, the Netherlands
[8]Lead contact
*Correspondence: b.v.steensel@nki.nl (B.v.S.), r.medema@nki.nl (R.H.M.)
https://doi.org/10.1016/j.celrep.2023.113124

SUMMARY

Acquired drug resistance is a major problem in the treatment of cancer. hTERT-immortalized, untransformed RPE-1 cells can acquire resistance to Taxol by derepressing the *ABCB1* gene, encoding for the multidrug transporter P-gP. Here, we investigate how the *ABCB1* gene is derepressed. *ABCB1* activation is associated with reduced H3K9 trimethylation, increased H3K27 acetylation, and *ABCB1* displacement from the nuclear lamina. While altering DNA methylation and H3K27 methylation had no major impact on *ABCB1* expression, nor did it promote resistance, disrupting the nuclear lamina component Lamin B Receptor did promote the acquisition of a Taxol-resistant phenotype in a subset of cells. CRISPRa-mediated gene activation supported the notion that lamina dissociation influences *ABCB1* derepression. We propose a model in which nuclear lamina dissociation of a repressed gene allows for its activation, implying that deregulation of the 3D genome topology could play an important role in tumor evolution and the acquisition of drug resistance.

INTRODUCTION

Chemotherapy is one of the main pillars of cancer treatment; however, chemotherapeutic drugs lose efficacy over time due to acquired drug resistance.[1,2] This acquired drug resistance can be the result of genetic mutations, as exemplified by mutations in receptor tyrosine kinases that cause resistance to tyrosine kinase inhibitors.[3,4] Alternatively, drug resistance can arise through elevated gene expression of the drug target itself, or by altered expression of proteins involved in drug metabolism.[5] The cause of this altered gene expression can be a genetic mutation or amplification of one of its upstream regulators, but changes in gene expression can also be due to epigenetic changes.[6,7] Well-known examples of the latter are changes in DNA methylation that result in altered gene expression in cancer.[8] How exactly these changes are induced during the evolution of drug resistance is currently unclear.

Here we have investigated the process of gene activation in the evolution of drug resistance in non-transformed immortalized human cells in culture. We have used derepression of the *ABCB1* gene as our model system to study gene regulation and acquired drug resistance.

Extensive research has shown that the *ABCB1* gene (also known as multidrug resistance gene or MDR) encoding the P-glycoprotein (P-gP) drug-efflux pump, is upregulated in many cancers cells exposed to increasing doses of Taxol and a variety of other chemotherapeutic drugs.[9,10] The contribution of P-gP to Taxol resistance in patients remains debated, with the possible exception of ovarian cancer, where it has been shown that Taxol resistance correlates with increased *ABCB1* expression.[11] In the same tumor type, *ABCB1* has been found fused with active promoters in Taxol-resistant samples.[12,13]

Prior studies have investigated the mechanisms of the *ABCB1* upregulation in cellular systems, and found that DNA-copy number amplifications of *ABCB1* locus can be linked to acquired chemoresistance.[14] Additionally, recent studies have shown that epigenetic alterations can also drive the upregulation of *ABCB1*. Particularly, several studies in Taxol-resistant cancer cell lines demonstrated that loss of repressive marks of heterochromatin, such as DNA methylation, in the regulatory region was associated with active transcription of the *ABCB1* gene.[15–18]

Although prior reports suggest a role for the methylation status in *ABCB1* regulation, the influence of the higher-order chromatin structure on gene expression and drug resistance is not yet

understood. In general, alterations in chromatin organization have been correlated to changes in gene expression,[19–23] and consequently, dysregulation of these may influence the functionality of the genome, leading to pathogenesis. It is well understood that the three-dimensional (3D) genome is maintained by a multilayer of structural units like chromosome territories, nuclear compartments, topological associating domains (TADs), and lamina associated domains (LADs). While chromosome compartments are proposed to be formed by block co-polymerization or micro-phase separation, TADs are often defined by CTCF and the cohesin complex.[24–26]

Several investigations have found alterations of the 3D genome involving TAD perturbations in cancer[26–28] as well as in autoimmune diseases and limb malformations.[29,30] Furthermore, a recent study reported mutations in CTCF-binding sites in 200 patient samples of colorectal cancer.[31] In addition to genomic organization in TADs, in the cell nuclei extensive chromatin regions are associated with the nuclear lamina (NL), which are mostly transcriptionally repressed[32–36] (reviewed in van Steensel and Belmont[37]). This raises the question of whether alterations in NL interactions could drive tumor evolution, and in particular, if such changes can lead to acquired drug resistance. Studies in *Drosophila* suggest that depletion of NL components alters gene expression of several chromatin regions, leading to defective cell differentiation.[38–40] However, in the context of drug resistance, it has not yet been examined whether 3D genome disorganization and detachment from the NL could be a potential mechanism of gene re-activation and consequently chemoresistance.

In order to explore novel mechanisms of gene re-activation and Taxol resistance, we generated Taxol-resistant cell lines derived from hTERT-immortalized, untransformed RPE-1 (RPE) cells. Consistent with our previous work,[41] we find that these cells become resistant to Taxol through re-activation of the *ABCB1* gene. In Taxol-sensitive cells, *ABCB1* is located in an LAD together with other inactive genes. We show that modifying chromatin marks by drug inhibition of DNA and histone-methyltransferase enzymes does not have a significant effect on the *ABCB1* expression. In addition to the observed changes in chromatin modifications, we identify important changes of the 3D genome topology when comparing the Taxol-sensitive versus the Taxol-resistant lines, particularly in the NL interactions. Furthermore, the disruption of Lamin B Receptor (*LBR*), an NL component, is able to derepress the locus leading to a Taxol-resistant phenotype. Therefore, this research provides a new understanding, from a high-order chromatin perspective, of how cells may gain resistance to chemotherapeutics such as Taxol.

RESULTS

Transcriptional activation of *ABCB1* drives Taxol resistance in RPE-TxR

In order to gain more insight into the processes that can lead to acquired drug resistance, we explored the molecular mechanism underlying *ABCB1* upregulation in the context of chemotherapy resistance. We made use of a previously described Taxol-resistant cell line derived from hTERT-immortalized, untransformed RPE-1 cells obtained after prolonged exposure to increasing doses of Taxol (RPE-Taxol resistant, RPE-TxR).[41] The RPE-TxR cell line is a polyclonal population of cells that acquired Taxol resistance during the drug-selection process. The generated cell line could proliferate under a Taxol concentration 20-fold higher than the parental RPE-1 (RPE-Taxol sensitive, RPE-TxS) (Figures 1A and 1B). Inhibition of the drug-efflux pump P-gP, by Tariquidar showed a re-sensitization of the RPE-TxR, indicating that Pg-P mediates resistance to Taxol in this cell line (Figures 1A and 1B).[41] We independently generated additional Taxol-resistant RPE polyclonal cell lines (TxR-3 and TxR-4) and confirmed that P-gP expression also conferred Taxol resistance in these lines (Figures S1A and S1B). To interrogate whether enhanced P-gP protein expression was due to transcriptional activation of the *ABCB1* gene, which encodes for P-gP, we performed RT-qPCR analysis and observed that the mRNA level of *ABCB1* was increased in all of these polyclonal lines (Figures 1C and S1C). In addition, we performed single-molecule RNA FISH (smRNA FISH) by generating a fluorescently labeled DNA probe targeting *ABCB1* intronic regions. This allows the visualization of nascent mRNAs, which enables the direct visualization of active transcription sites in the nucleus.[42] smRNA FISH revealed an increased number of active *ABCB1* transcription sites (TSs) in RPE-TxR compared with RPE-TxS (Figures 1D and 1E), indicating that *de novo* transcription was taking place in RPE-TxR. In order to confirm that *ABCB1* transcriptional activation was causal to Taxol resistance, we performed CRISPR interference (CRISPRi) experiments in RPE-TxR cells. Indeed, transcriptional downregulation of the *ABCB1* gene in RPE-TxR cells resulted in re-sensitization to Taxol (Figures S1D–S1G). Taken together, we corroborate in three independently generated cell populations that the major mechanism underlying acquired Taxol resistance in RPE-1 cells is through transcriptional activation of the *ABCB1* gene.

Chromosome 7 amplification is not sufficient to activate *ABCB1*

It is well described that genetic rearrangements and DNA mutations can lead to *ABCB1* transcriptional activation.[13,43,44] To understand whether this was the mechanism of *ABCB1* gene re-activation in RPE-TxR cells, we set out to analyze the *ABCB1* locus in this cell population. For this, we performed copy number analysis in both RPE-TxS and RPE-TxR cells. Interestingly, chromosome 7, where *ABCB1* is located, was amplified in a subset of TxR cells (Figure 2A). We therefore assessed whether *ABCB1* gene amplification in RPE-1 cells was sufficient to promote *ABCB1* upregulation and Taxol resistance. We performed Taxol-tolerance assays in a clonal cell line with three copies of chromosome 7, where *ABCB1* is located (Clone 20, Figure 2B). Strikingly, *ABCB1* amplification did not lead to increased mRNA levels or acquired Taxol resistance (Figures 2C–2E). This suggests that in order for RPE-1 cells to acquire Taxol resistance, rather than increased copies of *ABCB1*, other modifications are required.

ABCB1 gene activation in RPE-TxR is associated with changes in chromatin modifications and DNA contacts at the ABCB1 locus

To further understand the mechanism of *ABCB1* upregulation in RPE-TxR cells, we set out to investigate whether *ABCB1*

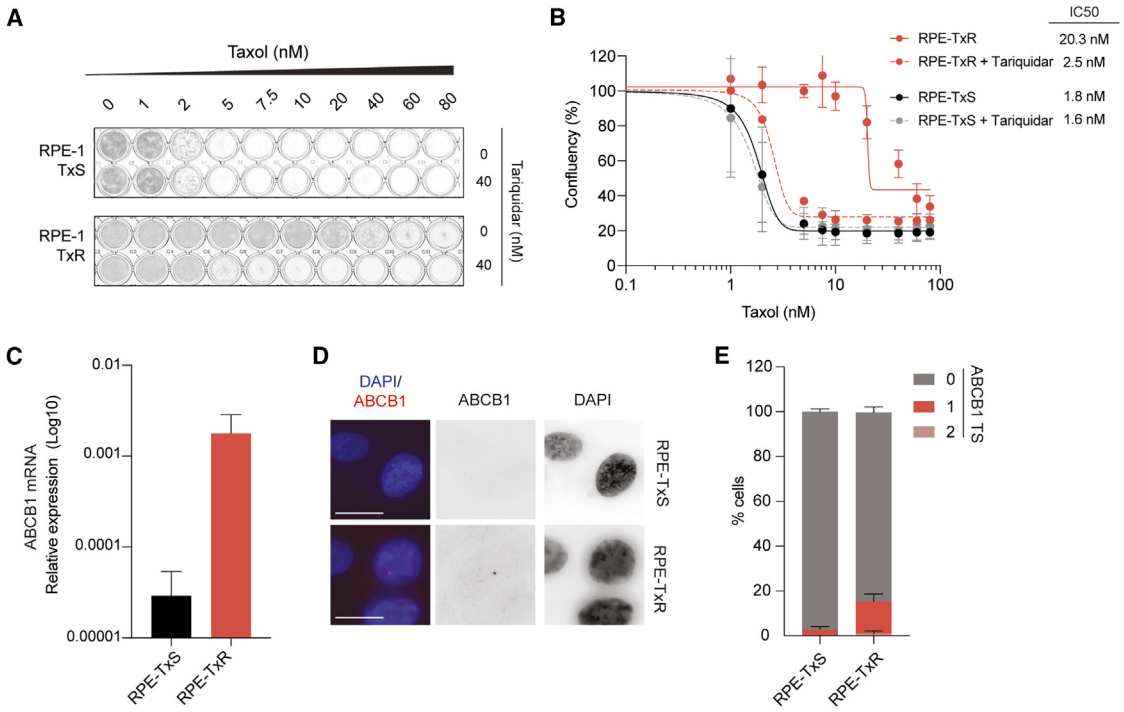

Figure 1. Transcriptional activation of *ABCB1* drives Taxol resistance in RPE-TxR

(A) Crystal violet staining of viability assay on Taxol-naïve RPE-TxS and resistant RPE-TxR cell lines.

(B) Relative survival plots of the RPE-TxS and RPE-TxR cell lines. Error bars show the average ± SD of three independent experiments (n = 3) and the calculated IC50. The curve was drawn from the log(inhibitor) vs. response equation *Y = Bottom + (Top − Bottom)/(1 + 10^(X-LogIC50))*.

(C) *ABCB1* mRNA levels determined by qRT-PCR and normalized to *GAPDH* expression levels. Error bars show the average ± SD of three independent experiments (n = 3). The y axis is shown in logarithmic scale.

(D) Representative smRNA-FISH images of RPE-TxS and RPE-TxR for the *ABCB1* gene and DAPI. The images are projections of 0.5-μm sections and a total 5 μm in thickness. Scale bar, 15 μm.

(E) Quantification of the number of *ABCB1* transcription sites (TS) found per cell. Error bars show the average ± SD of three independent experiments (n = 3), 60 cells per replicate and condition.

expression is accompanied by changes in chromatin modifications at the *ABCB1* locus. To this end, we analyzed histone marks and DNA methylation patterns by chromatin immunoprecipitation and bisulfite treatment, respectively, followed by massive parallel sequencing. We found that, compared with RPE-TxS, RPE-TxR lost the repressive modification H3K9me3 and gained active marks (H3K27ac and H2AZ) in the promoter region of the *ABCB1* gene (Figures 3A–3C). In addition, a *de novo* peak of H3K27ac upstream of *ABCB1* was detected in RPE-TxR (Figure 3B, arrow, and Figure S2A). Bisulfite sequencing analysis showed no significant decrease on DNA methylation at the *ABCB1* promoter in RPE-TxR (Figure S2B). Analysis of previously published Hi-C data for RPE-1 cells[45] demonstrated that *ABCB1* is found in a TAD together with two other genes, *ABCB4* and *RUNDC3B* (Figure S2C). Interestingly, in addition to the 7-fold increase observed in the *ABCB1* mRNA levels, the RNA-sequencing experiments also showed an upregulation of *ABCB4* and *RUNDC3B* in RPE-TxR (Figure S2D). The same was seen in the additional independently generated RPE-1-derived Taxol-resistant cell lines (TxR-3 and TxR-4) (Figures S2E and S2F). Because changes in gene regulation are often associated with local changes in chromosome folding,[46] we performed targeted locus amplification (TLA) in RPE-TxS and RPE-TxR. This strategy allows to selectively amplify and sequence DNA on the basis of the crosslinking of physically proximal sequences similarly to 4C-seq.[47] We identified changes in chromatin contacts of the *ABCB1* locus in RPE-TxR compared with RPE-TxS (Figure 3D). In RPE-TxS, *ABCB1* preferentially interacts with regions enriched for H3K9me3 and low for H3K36me3, associated with heterochromatin and transcriptionally active regions, respectively[48,49] (Figures 3A, 3D, and S2G). However, in RPE-TxR, contacts also occurred in less enriched H3K9me3 domains. Moreover, new interactions with the promoters of the transcribed genes *SLC25A40*, *CROT, DMTF1,* and *TMEM243* were observed, marked by H3K36me3 and H3K4me3 (Figures 3D, S2G, and S2H). These new interactions were also enriched on H3K4me1 and H3K27ac, enhancer-associated marks[50] (Figure S2G), suggesting that the *ABCB1* gene could potentially be regulated by proximal enhancers. Therefore, we conclude that chromatin marks undergo major changes at the *ABCB1* locus during the acquisition of Taxol resistance. This is also the case for *ABCB1* DNA interactions, suggesting that genes are more likely to interact with regions with similar chromatin nature.

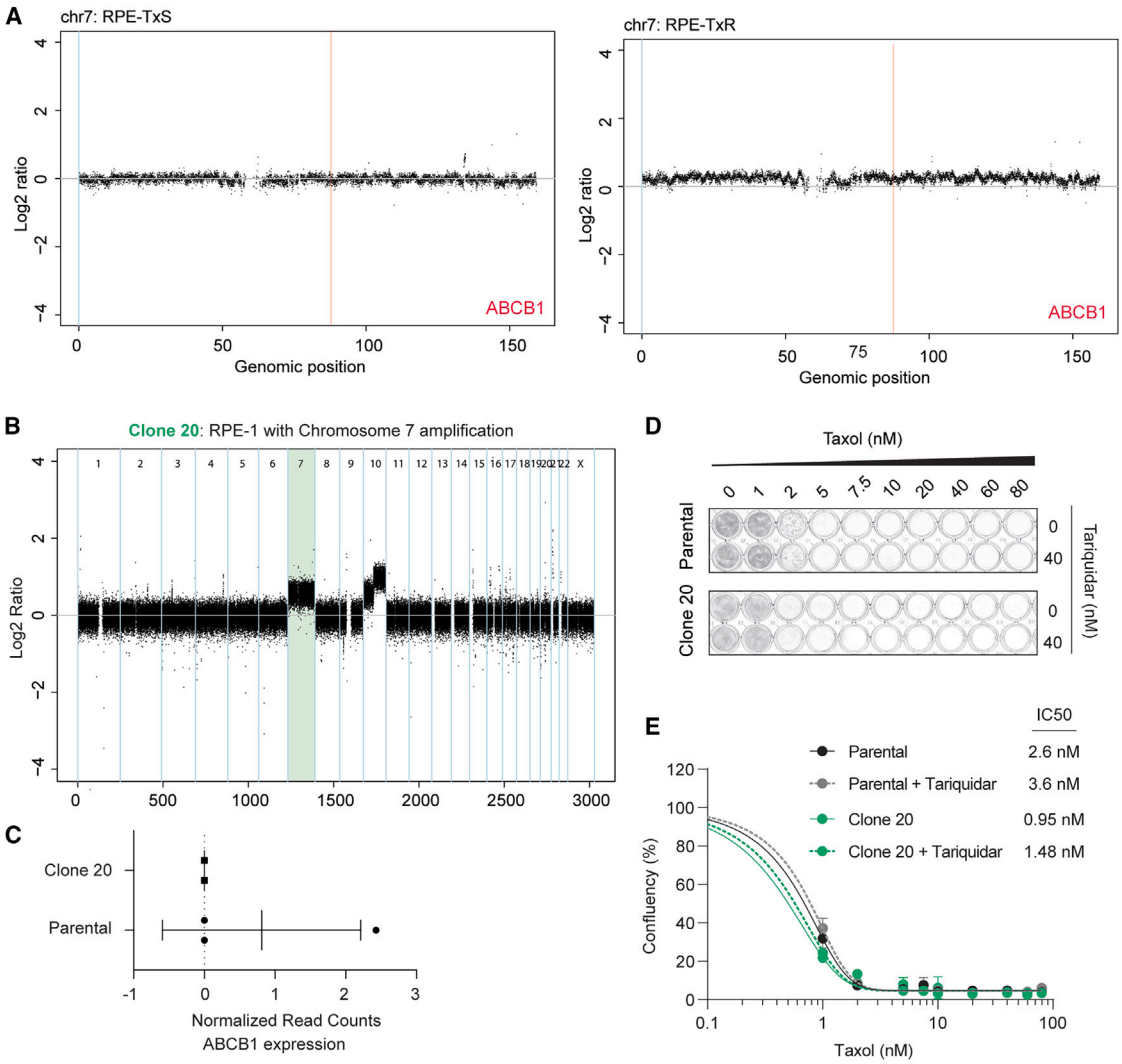

Figure 2. Chromosome 7 amplification is not sufficient to activate *ABCB1*

(A) Copy number variation analysis in RPE-1 Taxol-sensitive and RPE-1 Taxol-resistant cells. Chr7 region is shown and *ABCB1* location is depicted in red.

(B) Copy number analysis showing all chromosomes in RPE-1 cells (Clone 20). Chromosome 7, with one extra copy, is highlighted in green, where *ABCB1* is found. Data are obtained from a single replicate.

(C) RNA-sequencing data showing the normalized read counts of the *ABCB1* gene in Parental vs. Clone 20 from (B).

(D) Crystal violet staining of viability assay on Clone 20 and RPE-1 Parental cells.

(E) Relative survival plots of the Parental and Clone 20 cell lines. Error bars show the average ± SD of two independent experiments (n = 2) and the calculated IC50. The curve was drawn from the log(inhibitor) vs. response equation *Y = Bottom + (Top − Bottom)/(1 + 10^(X-LogIC50))*.

ABCB1 gene activation in RPE-TxR is associated with detachment from the NL

As gene silencing has been linked to association with the NL,[37] we also performed pA-DamID of Lamin B2. This is an antibody-based variant of the DamID technology that allows visualization of genome-NL interactions with high temporal resolution.[51] We observed that in RPE-TxS the pA-DamID signal intensity of the *ABCB1* locus was very high (Figure 4A, blue curve TxS profile), indicating that it is in an LAD. In contrast, in RPE-TxR cells, the pA-DamID signal intensity in the *ABCB1* region was greatly reduced (Figure 4A, red curve TxR profile), indicating that a major NL detachment of the region containing *ABCB1* and its neighboring has taken place during the acquisition of drug resistance. Interestingly, *SLC25A40*, *CROT, DMTF1,* and *TMEM243,* which had higher contact interactions with *ABCB1* in RPE-TxR (Figure 3D, TLA analysis), were also found detached from the NL in RPE-TxS (Figure 4A). This suggests that when *ABCB1* loses its interaction with the NL, it tends to gain interactions with other inter-LAD (iLAD) genes. In addition to this, we could also observe a possible "compensatory" movement of the regions farther from the *ABCB1* locus, which increased NL contacts in the Taxol-resistant cell lines (Figure 4A, red curve TxR profile). Possibly the site that is left vacant by the release of the *ABCB1* locus from the lamina tends to establish (weak)

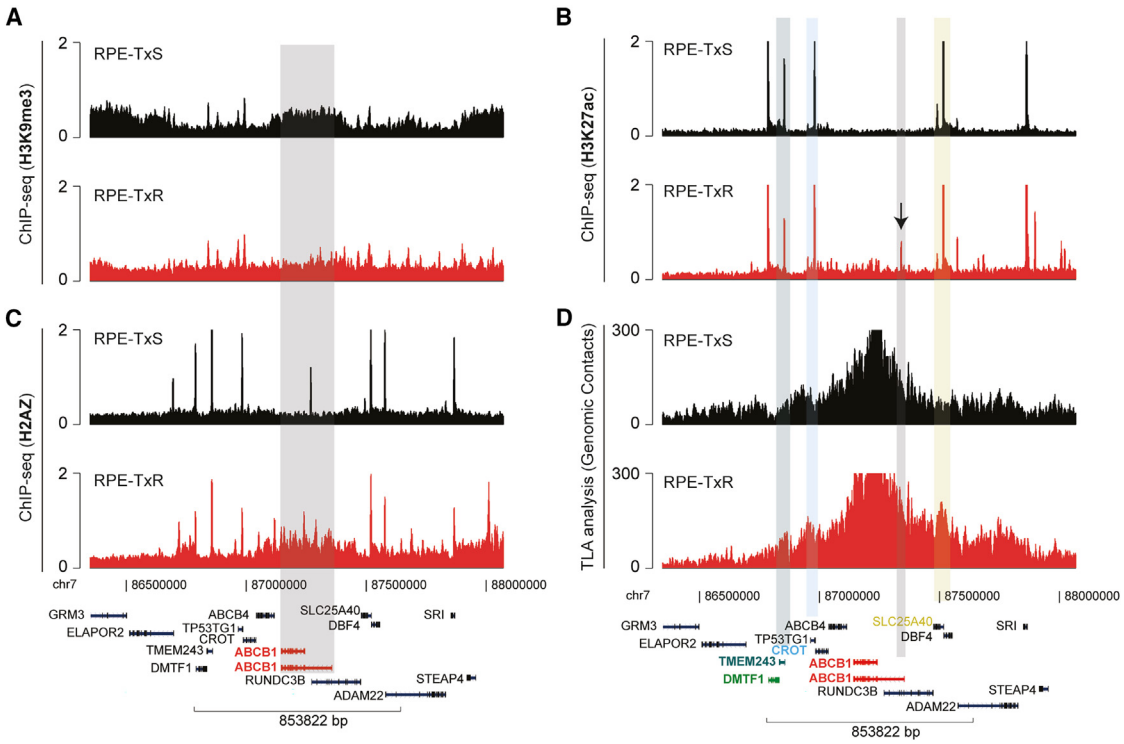

Figure 3. *ABCB1* gene activation in RPE-TxR is associated with changes in chromatin modifications and 3D genome

(A) Normalized ChIP signal for H3K9me3 (B) H3K27ac or (C) H2AZ in RPE-TxS and TxR cell lines. In H3K27ac an arrow shows a *de novo* peak in the *ABCB1* region. Gray bars show the region where *ABCB1* is located and the observed changes in histone marks. *ABCB1* gene is labeled in red, two isoforms are depicted. ChIP data show read-based normalization signal based on pooled biological replicates (n = 2) (see STAR Methods for details).

(D) TLA analysis of the *ABCB1* gene in RPE-TxS (top) and RPE-TxR (bottom) (gene annotation hg19). Sequencing expanding regions immediately neighboring the *ABCB1* gene have higher coverage. Colored lines show new contacts formed in RPE-TxR with the indicated colored genes. Data are obtained from a single replicate.

interactions with whatever is closest. In order to measure the overall changes in lamina interactions between the resistant and the sensitive cell lines, we quantified the pA-DamID signals. We used genes as units, and we calculated an NL association score for every gene starting from GATC counts (see STAR Methods section). We then correlated the pA-DamID signal between RPE-TxS and RPE-TxR (Figure 4B). We could confirm *ABCB1* as one of the genes losing LaminB2 signal in the TxR cells (Figure 4B). Interestingly, even though we found most genes maintaining their pA-DamID signal (R = 0.89), there was a significant number of other genes losing pA-DamID interactions in the Taxol-resistant cell line.

In order to detect changes in NL association at single-cell resolution, we generated RPE-1 cells with a fluorescent endogenous label at the *ABCB1* locus using the ANCHOR3 system.[53] The ANCHOR3-system relies in the stable integration of a short, non-repetitive sequence (ANCH) that is placed adjacent to the locus of interest. The ANCH-sequence can then be recognized by OR3 proteins that are fused to fluorescent eGFP and accumulate at the ANCH-sequence to form a focus[53] (Figure 4C). We generated and validated RPE-1 cells, which had the ANCH endogenously integrated in *ABCB1,* and stably expressed OR3-GFP (Figures S3A–S3C). From these cells, we derived a new Taxol-resistant cell line resistant to similar doses of Taxol as the original TxR (Figures 1A and S3B–S3D). In order to measure the distance from *ABCB1* to the NL in TxS and TxR ANCHOR3 cells, we performed immunofluorescence with a LaminB1 antibody (Figures 4D and S3E). Based on the fluorescent signal of LaminB1, we were able to segment the NL as an iso-surface in 3D (Figure S3F). By additionally segmenting the ANCHOR3-foci of the individual cells as iso-surfaces, we were able to measure the shortest distance between the nuclear periphery and its corresponding ANCHOR3-foci in 3D (Figures 4E, S3E, and S3F). Strikingly, we could observe that in ANCHOR3 TxR cells, *ABCB1* was located farther away from the NL compared with TxS (Figure 4E). It is significant to note that some of the ANCHOR3 TxR cells had two ANCHOR3-foci, suggesting that *ABCB1* has been amplified, consistent with what we observe in Figure 2A (Figure S3E). Importantly, by pA-DamID, we could confirm that four other independently generated Taxol-resistant cell lines (TxR-3, TxR-4, TxR-5, and TxR.6), even though variable scores, also had significantly lower interactions with the NL in the *ABCB1* locus (Figures S3G and S3H). Overall, these results indicate that a local rewiring of NL interactions occurs in the *ABCB1* genomic region in the RPE-1 Taxol-resistant cells.

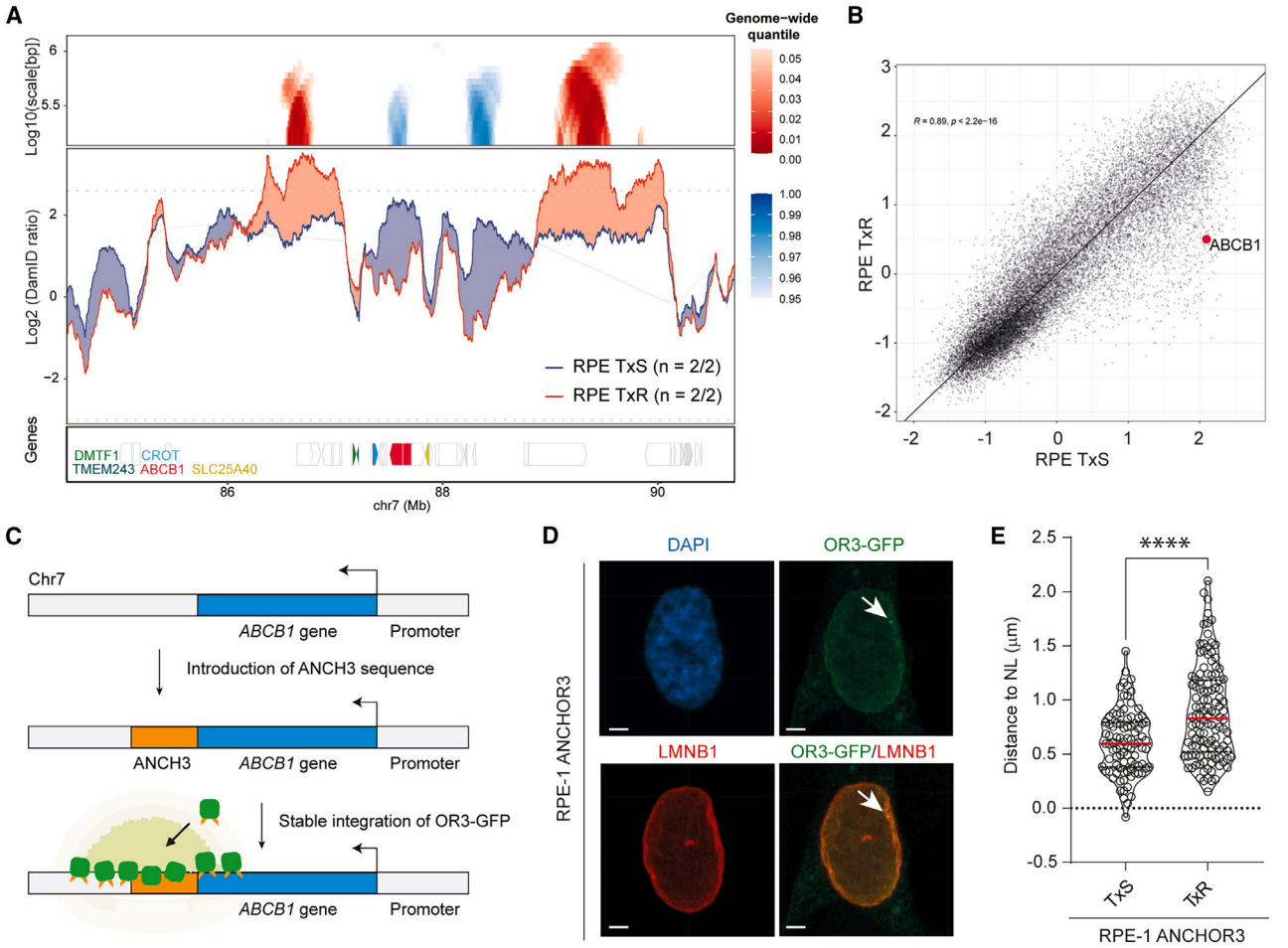

Figure 4. *ABCB1* gene activation in RPE-TxR is associated with detachment from the NL

(A) Change in NL interactions of *ABCB1* and flanking regions in RPE-TxR compared with RPE-TxS, detected by pA-DamID.[51] Data are visualized as in Brueckner et al.[52] Bottom panels: gene annotation track (hg38); *ABCB1* gene is marked in red. Middle panels: pA-DamID tracks of NL interactions in Taxol-sensitive cells (TxS, blue line) and Taxol-resistant cells (TxR, red line). n indicates the number of independent biological replicates that were combined. Noise was suppressed by a running mean filter of indicated window size. Shading between the lines corresponds to the color of the sample with the highest value. Dashlines mark the fifth and 95th percentiles of genome-wide pA-DamID values. Top panels: domainograms; for every window of indicated size (vertical axis) and centered on a genomic position (horizontal axis), the pixel shade indicates the rank of the change in pA-DamID score (experimental [TxR] minus control [TxS]) compared with the genome-wide changes in pA-DamID scores across all possible windows of the same size. Only significant changes (within the fifth or the 95th genome-wide quantiles) are colored. Blue: pA-DamID score is highest in control samples; red: pA-DamID score is highest in experimental samples. (Color key genome-wide quantile is shown on the right of the panel.)

(B) pA-DamID signals were quantified as described in the method section using genes as units extended of ± 10 kb (n = 2). Every point represents a single gene; *ABCB1* is highlighted in red. Graphs represent the pA-DamID *Z* score signal correlated between Taxol-resistant cells and Taxol-sensitive cells. The two cell lines show a strong overall correlation (Pearson correlation coefficient R = 0.89), but the *ABCB1* gene shows a marked difference in pA-DamID signal between the two cell lines.

(C) Schematic representation of the ANCHOR3-system[53] to visualize the endogenous *ABCB1* locus.

(D) Z-projection example image of immunofluorescence staining with LaminB1 antibody and the OR3-ABCB1 focus. Scale bar, 2 μm.

(E) Quantification of the shortest distance in three-dimensional space from the ANCHOR3-ABCB1 foci to the nuclear lamina in RPE-1 ANCHOR3 TxS and TxR. The analysis is performed as described in STAR Methods. Red bar represents the median of n = 91 TxS and n = 118 TxR cells from three independent experiments, ****p < 0.0001, Mann-Whitney test.

Transition to Taxol resistance is not primarily driven by repressive chromatin modifications of the *ABCB1* genomic locus

In order to test whether altering the chromatin modifications of the *ABCB1* locus is sufficient to derepress *ABCB1* in RPE-TxS, we made use of different drugs to perturb the epigenetic landscape. The addition of 5-aza deoxycytidine (5-AZA) for 24 h was able to reduce the levels of DNMT1, the enzyme responsible for DNA methylation deposition (Figures 5A, 5B, and S4A). In the *ABCB1* promoter, a decrease of DNA methylation was also observed upon DNMT1i (Figures S4B and S4C). A similar trend for the levels of H3K27-trimethylation occurred when treating

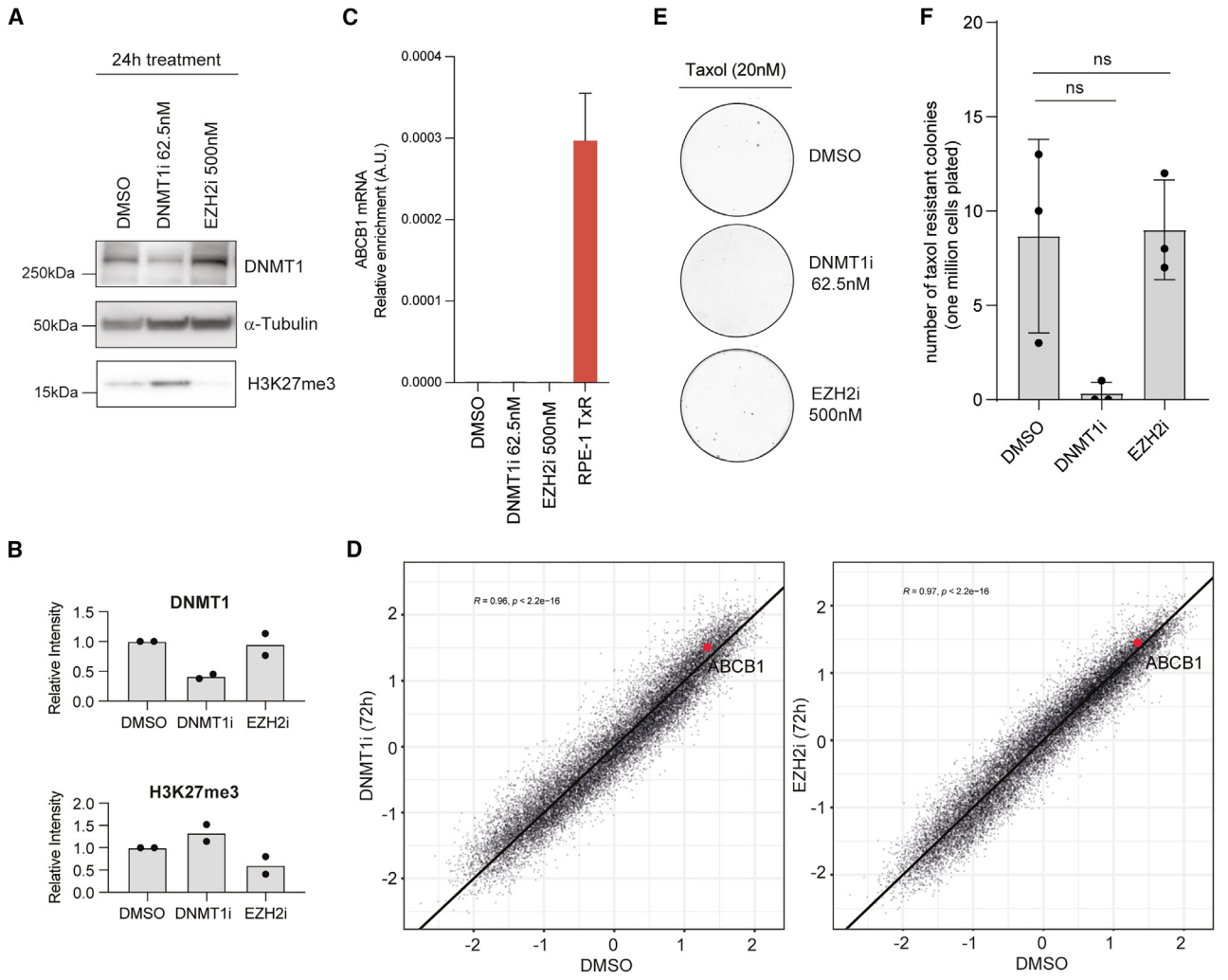

Figure 5. Transition to Taxol resistance is not primarily driven by repressive chromatin modifications of *ABCB1* genomic locus

(A) Western blot showing the levels of the chromatin proteins and controls (a-TUBB) upon treatment with the indicated epigenetic drugs with for 24 h.

(B) Western blot quantification over TUBB control and normalized to DMSO. Each dot represents an independent western blot experiment (n = 2).

(C) *ABCB1* mRNA levels determined by qRT-PCR and normalized to *GAPDH* expression levels upon drug addition and RPE-TxR as a control for *ABCB1* expression, Error bars show the SD of three technical replicates.

(D) pA-DamID *Z* score signals were quantified using genes as units as Figure 4B (n = 2). Every point represents a single gene; *ABCB1* is highlighted in red. Graphs represent the pA-DamID signal correlated between DMSO vs. 5AZA 62.5 nM 72 h- (left) and DMSO vs. GSK126 500 nM 72 h-treated cells (right). Pearson correlation: 0.96 and 0.97, respectively.

(E) Crystal violet staining of colony-formation assay under 20 nM of Taxol and the corresponding chromatin drug in RPE-1 iCut WT cells. One million cells were plated per condition.

(F) Quantification of the number of Taxol-resistant colonies from (E). Error bars show the average ± SD of independent experiments (n = 3). ns, p > 0.05, Mann-Whitney test.

cells with GSK126 (EZH2 inhibitor), which interferes with H3K27me3 deposition (Figures 5A, 5B, and S4D). Under these treatments, we performed RT-qPCR in RPE-TxS to check *ABCB1* expression levels. We observed that both drugs were unable to induce transcription of the *ABCB1* gene (Figure 5C). We next performed pA-DamID under the same drug treatments in order to assess *ABCB1* NL contacts (Figure 5D). Correlations between the pA-DamID signal between DMSO-treated and DNMTi or EZH2i did not show any change in NL interactions, including the *ABCB1* locus (Figure 5D). In order to assess the relative position of *ABCB1* within the nucleus at single-cell resolution, we also treated RPE-1 ANCHOR3 cells with chromatin-perturbing drugs (Figures S4F and S4G). In this set up, we could also not observe a significant increase in distance between *ABCB1* and the NL (Figure S4G). Thus, altering the levels of the H3K27-methyltransferase EZH2 or the DNA methyltransferase DNMT1 is not sufficient to perturb the localization of *ABCB1* within the nucleus or to derepress the gene.

We next asked if altering H3K27-trimethylation or DNA methylation at the *ABCB1* promotor is sufficient to precondition the

locus for derepression. To this end, we performed colony-formation assays using a combination of these drugs and Taxol. For the chromatin-modifying drugs, we determined a dose that did not induce a proliferation defect (Figures S4A and S4H). We pre-treated RPE-TxS cells with DNMT1i or EZH2i for 24 h followed by an overnight co-treatment with 20 nM Taxol. Next morning the chromatin-modifying drugs were washed out and only 20 nM Taxol was present for 15 days. Neither the DNMT1 nor EZH2 inhibitor were able to increase the number of Taxol-resistant colonies (Figures 5E and 5F). In fact, DNMT1i in combination with Taxol led to a decrease in Taxol-resistant colonies compared with the DMSO control (Figures 5E and 5F). To boost the drug efficacy, we treated RPE-TxS cells for 72 h with a higher dose of DNMT1i and maintained the same EZH2i dose. Even though we observed protein depletion by western blot (Figure S4I), *ABCB1* mRNA levels quantified by qPCR remained similar to the DMSO-treated condition (Figure S4J). It has been suggested that alterations in H3K9me2 by the G9a inhibitor affect LAD organization.[54,55] Therefore, we also inhibited the H3K9me2 methyltransferase G9a with BIX-01294 followed by RT-qPCR analysis and NL interactions assessment. Like DNMT1 and EZH2 inhibitors, the G9ai was not able to increase *ABCB1* mRNA levels or displace *ABCB1* from the NL (Figures S4A and S4E–S4K). Unfortunately, we were unable to reliably measure levels of H3K9me2 by chromatin immunoprecipitation (ChIP), so it is not clear if this treatment results in altered H3K9me2 levels at the ABCB1 locus. Also, due to the toxicity of this inhibitor following 24 h of treatment (Figure S4H), we could not assess colony formation under Taxol pressure. Nonetheless, these data do suggest that the disruption of chromatin-modifying enzymes by drug inhibition is unable to trigger activation of *ABCB1* gene transcription in RPE-1 cells, and thereby remain Taxol-sensitive.

Differentially expressed transcription factors do not seem to play a role in *ABCB1* expression and acquisition of Taxol resistance

We next investigated whether potential upregulation of transcription factors (TFs) in RPE-TxR cells could be responsible for initiation of *ABCB1* gene expression, and thereby change local chromatin modifications and 3D genome organization at the *ABCB1* locus. We first performed motif scan to identify the potential TFs binding to the promoters of the two *ABCB1* isoforms. Subsequently, we hypothesized that gain of Taxol resistance may be caused by aberrant expression of some of these TF interactors, and therefore we identified all the differentially expressed TF binders of the two promoters in RPE-TxR compared with RPE-TxS using mRNA sequencing (Figure S5A). To further narrow down our searching, we speculated that the TFs responsible for the *ABCB1* derepression may potentially play an activation role for other upregulated genes in the resistant cells. Hence, we also performed a motif analysis for the promoters of all the upregulated genes in RPE-TxR in order to identify general promoter activators in the resistant cell line. We mainly found significantly enriched motifs belonging to the POU and LHX TF homeodomain family (Figures S5B and S5C). This implies that these TFs may potentially be involved in the upregulation of many genes on the RPE-TxR cell lines, including *ABCB1*. To test this, we overexpressed *POU3F2*, *LHX6,* and *ZIC5,* which showed a clear upregulation in the resistant cells (Figure S5A), in the Taxol-sensitive parental RPE cells. To that aim, we used the Cas9-VP64-transcription activation system (CRISPRa) to assess whether this would recapitulate *ABCB1* activation in the resistant cell line. Even though we observed by RT-qPCR a significant increase of mRNA expression of the three TFs, similar to the level of upregulation in RPE-TxR (Figure S5D), this did not result in a Taxol-resistant phenotype (Figures S5E and S5F). More importantly, downregulation of these TFs in RPE-TxR did not perturb the Taxol-resistant phenotype (Figures S5G–S5I), indicating that *POU3F2*, *LHX6,* and *ZIC5* are not required to maintain increased *ABCB1* gene transcription in RPE-TxR cells. However, we cannot exclude that they could be necessary to establish the initial transcriptional upregulation. Also, it remains possible that there is a transcription factor upregulated that is responsible for *ABCB1* re-activation that our analysis failed to pick up.

ABCB1 upregulation in RPE-TxR is not caused by direct activation of the promoter by *trans*-acting factors

We next wondered whether RPE-TxR cells upregulated additional TF that could lead to the activation of the *ABCB1* promoter. Therefore, to further exclude TF activation as the initial trigger for *ABCB1* gene activation, we carried out a luciferase reporter assay to assess the *ABCB1* promoter activity in RPE-1 Taxol-sensitive (TxS) and Taxol-resistant (TxR3-4) cells. To this end, the *ABCB1* promoter was cloned in a pGL3-basic vector followed by transfection into RPE-TxS or RPE-TxR. If similar luciferase activity was observed between cell lines, that would indicate that there are not differentially expressed *trans*-acting factors that lead to *ABCB1* promoter activation. However, if there is an increase of luciferase activity in RPE-TxR, a *trans*-acting factor may be upregulated, therefore inducing *ABCB1* promoter activation. Activity of the *ABCB1* promoter was relatively low compared with the pGL3-promoter plasmid, but more importantly, we did not observe an increase of luciferase activity in TxR cells compared with TxS (Figure S6A). This suggests that RPE-1 TxR cells do not have a distinct transcriptional program or differentially expressed TFs that could activate the *ABCB1* promoter. Instead, the 3D genome topology may be the determining factor for the *ABCB1* expression. Therefore, we hypothesized that NL detachment observed in RPE-TxR potentially could be a first step toward acquired drug resistance, subsequently allowing recruitment of available TFs leading to transcription activation of the *ABCB1* gene.

LBR depletion facilitates acquisition of Taxol resistance

To further understand the importance of NL components in *ABCB1* gene expression, we generated different knockouts (KOs) of NL proteins using CRISPR-Cas9 technology in RPE-1 Cas9 cells (RPE-1 iCut).[56] We obtained a high cutting efficiency of the Lamin B Receptor (*LBR*) gene in a polyclonal cell population (Figure 6A). Moreover, we could confirm by western blotting that *LBR* was depleted effectively (Figure 6B). To explore the reorganization of the LAD landscape that takes place upon *LBR* depletion, we performed pA-DamID in the polyclonal RPE-1 *LBR* KO cells. No significant rewiring of the genomic

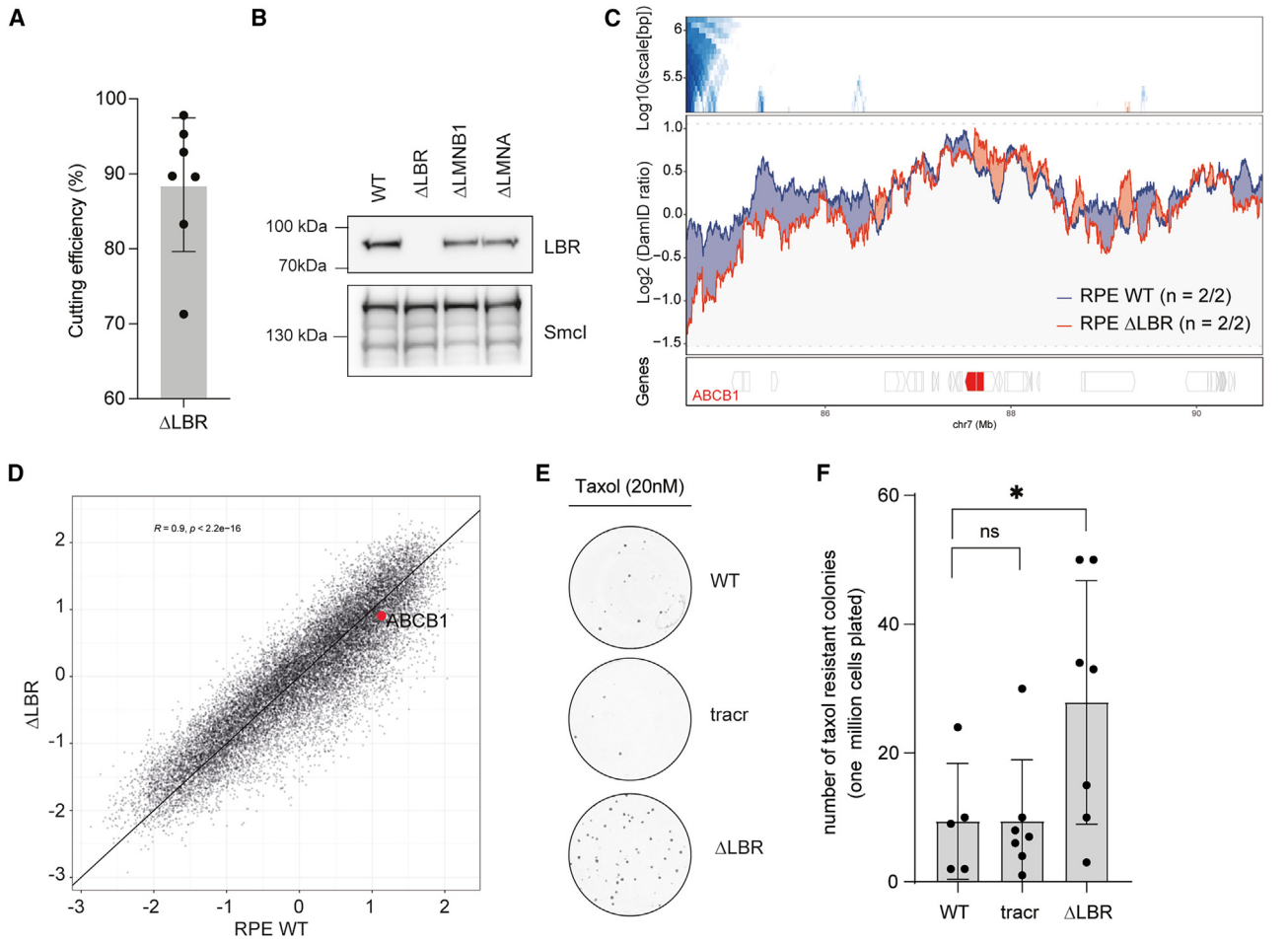

Figure 6. *LBR* depletion facilitates acquisition of Taxol resistance

(A) Percentage of disrupted sequence (cutting efficiency) in RPE-1 iCut cells transfected with crRNAs targeting the *LBR* gene and using TIDE analysis. Black dots show an independent biological replicate. Error bars show the SD.

(B) Western blot showing the levels of *LBR* and control (SMC1) proteins 7 days after transfection of *LBR, LMNA,* or *LMNB1* crRNAs.

(C) Change in NL interactions of *ABCB1* and flanking regions in *LBR* KO (crRNA-*LBR*) compared with RPE WT as analyzed in Figure 4A. Color key domainogram as in Figure 4A.

(D) pA-DamID *Z* score signals were quantified using genes as units (n = 2) as in Figure 4B. Every point represents a single gene; *ABCB1* is highlighted in red. Graphs represent the pA-DamID *Z* score signal correlated between *LBR* KO and RPE WT. Pearson correlation: 0.9.

(E) Crystal violet staining of colony-formation assay under 20 nM of Taxol in RPE-1 iCut WT cells, transfected with only tracrRNA or tracrRNA and crRNA-*LBR* (*LBR* KO). One million cells were plated per condition.

(F) Quantification of the number of Taxol-resistant colonies from (E). Error bars show the average ± SD of WT (n = 5), tracr (n = 7), and crRNA-*LBR* (n = 7) replicates. WT vs. *LBR* *p = 0.049, tracr vs. *LBR* *p = 0.041, Mann-Whitney test.

region containing the *ABCB1* locus from the NL was detected in this polyclonal population by pA-DamID (Figure 6C). *ABCB1* pA-DamID signal in *LBR* KO compared with wild type (WT) was not significantly changing (Figures 6C and 6D). In addition, the overall *ABCB1* mRNA levels were not increased in the *LBR* KO population (Figure S6B). Complete depletion of Lamin B1 (*LMNB1*) or Lamin A/C (*LMNA*), structural and supporting components of the NL, had no obvious effect on *ABCB1* transcriptional regulation or *ABCB1* NL detachment (Figures S6B–S6D). Several genes, mainly with an intermediate lamina association score, showed decrease in NL association following LMNA/C KO. Interestingly, genes with high lamina association score become even more associated with the NL, including *ABCB1* (Figure S6D). This suggests a reorganization of DNA-NL contacts following Lamin A/C ablation genome-wide, in agreement with previous findings.[57–59]

We next asked whether perturbations in NL components were sufficient to precondition *ABCB1* for derepression to precondition cells for the acquisition of Taxol resistance. Seven days after the KO generation, we performed colony-formation assays using 20 nM of Taxol. Upon *LBR* depletion, we observed an increase in the number of Taxol-resistant colonies in multiple independent experiments (Figures 6E and 6F). This implies that the loss of *LBR* can facilitate derepression of the *ABCB1* gene when cells are exposed to Taxol. It should be noted, however, that only a

small fraction of cells in the population acquired Taxol resistance (Figure 6E), and the absolute number of Taxol-resistant colonies we obtained varied from experiment to experiment, suggesting the importance of other factors in activating the *ABCB1* gene. Nevertheless, the number of Taxol-resistant clones is significantly higher in *LBR* KO cells than what we observe in the parental lines. This was not the case for Lamin A/C- and Lamin B1-depleted cells (Figures S6E and S6F).

In order to investigate whether depletion of *LBR* induced *ABCB1* upregulation in other *in vitro* models, we performed RNA interference experiments in various cancer cell lines. We selected a triple-negative breast cancer cell line (MDA-MB-231), a head-and-neck squamous cell carcinoma (FaDu), and a lung adenocarcinoma cell line (A549). Using RT-qPCR analysis, we found that MDA-MB-231 and FaDu had slightly higher *ABCB1* mRNA levels than RPE-1 cells. In contrast, the *ABCB1* mRNA levels detected in A549 were considerably increased (Figure S7A). Depletion of *LBR* by small interfering RNA (siRNA) led to a decrease of *LBR* protein levels 48 h post-transfection in all cell lines (Figure S7B). We also assessed whether the siRNAs were affecting normal cell proliferation, which showed minimal effects (Figure S7C). After 48 h, colony-formation assays under different concentrations of Taxol for each of the cell lines were performed. As control, we confirmed that depletion of *LBR* by siRNA led to an increase in the number of Taxol-resistant colonies in RPE-1 cells (Figures S7D and S7E). As expected, based on the high level of *ABCB1* expression, A549 cells were resistant to high levels of Taxol, and depletion of *LBR* had minimal effects (Figures S7D and S7E). The effect of *LBR* depletion in MDA-MB-231 also resulted in increased numbers of Taxol-resistant colonies, similar to what we observe in RPE-1 cells (Figures S7D and S7E). *LBR* depletion in FaDu cells resulted in a decrease of Taxol-resistant colonies (Figures S7D and S7E). These data imply that loss of lamina interaction is a key event for the derepression of *ABCB1*, but additional factors are required to achieve complete derepression.

Based on these data, we propose that in RPE-1 cells, and possibly across various other *in vitro* models, *LBR* may act as a regulator of the *ABCB1* gene expression and its depletion can contribute to acquired Taxol resistance. Additionally, these data suggest that NL association may act as a critical threshold that needs to be overcome in order to derepress a gene, and as such, loss of lamina association seems to represent a key step in the process of transcriptional derepression.

Transcription-driven CRISPRa activation of neighboring genes can detach *ABCB1* from the NL and lead to Taxol resistance

To further explore the role of NL in ABCB1 regulation, we examined whether NL detachment would lead to *ABCB1* gene activation. It has been previously described that the CRISPRa induces detachment of genes from the NL, and in some instances this also causes detachment of flanking genes.[52] We therefore attempted to detach *ABCB1* from the NL by activation of its neighboring genes. We used CRISPRa to specifically activate the promoter of *ABCB1*, *ABCB4,* or *RUNDC3B* or a combination of the latter two (Figure 7A). Next, we performed Lamin-pA-DamID to map NL interactions (Figures 7B, 7C, S8A, and S8B). We observed that in control cells, *ABCB1* is located at the NL, together with the *ABCB4* and *RUNDC3B* genes (Figures 7B, 7C, S8A, and S8B, blue lines). As expected and showed in previous research,[52] upon CRISPRa single gene activation, local NL detachment was detected in the regulatory regions and most of the transcription units of these genes (Figures 7B, S8A and S8B, red line). Strikingly, simultaneous activation of *ABCB4* and *RUNDC3B* caused not only detachment of these two genes, but also of *ABCB1* (Figure 7C, red line). Next, we asked whether this was accompanied by upregulation of *ABCB1* expression. We observed that transcription activation of *ABCB1* by CRISPRa led to an expected increase of mRNA of *ABCB1* (Figure 7D). Surprisingly, activating *ABCB4*, *RUNDC3B,* or the combination via CRISPRa also triggered the activation of *ABCB1* (Figures 7D and S8C), and was accompanied by an increase in occurrence of Taxol-resistant colonies (Figures 7E and S8D–S8G). We next performed ChIP-qPCRs on the *ABCB1* regulatory region (P2) and observed a decrease in the H3K9me3 signal in both CRISPRa-*ABCB1* and CRISPRa *ABCB4-RUND3CB* compared with the CRISPRa parental cell line (Figures 7F and S8J). However, even though CRISPRa-*ABCB1* presented an enrichment of H3K27ac in the *ABCB1* promoter, the combination of *ABCB4* and *RUNDC3B* did not show this (Figures 7G and S8J). To rule out the possibility that the *ABCB1* transcription initiation by *ABCB4* and *RUNDC3B* was a consequence of cross-activation of the *ABCB1* promoter, we generated new single guide RNAs (sgRNAs) targeting upstream and downstream of the *ABCB1* regulatory regions (Figure S8K). We could confirm that these sgRNAs, even though in the same TAD as *ABCB1*, could not initiate transcriptional activation, as shown by RT-qPCR (Figure S8L). Therefore, we can conclude that *ABCB1* transcription is linked to loss of H3K9me3 and NL detachment, potentially caused by activation of *ABCB4* and *RUNDC3B* and not due to cross-activation of the sgRNAs. Also, these observations are compatible with a model in which NL detachment is a key step for gene activation driving acquired drug resistance. However, it should be noted that it is equally well possible that active transcription of neighboring genes, subsequently leading to NL detachment of the gene of interest, is what can trigger gene re-activation.

DISCUSSION

In this study we describe a novel mechanism by which cells can upregulate *ABCB1*, a gene involved in Taxol resistance. Our data provide the first direct link between 3D genome reorganization and drug resistance. We have shown that Taxol resistance of RPE-TxR cells can be entirely attributed to the activity of the P-gP drug-efflux pump.[41] In RPE-TxR, *ABCB1*, the gene encoding for P-gP, is upregulated through transcriptional activation. This transcriptional activation coincides with an enrichment of active histone marks and a depletion of repressive marks in the chromatin environment of the *ABCB1* promoter. However, directly altering the chromatin landscape in RPE-TxS cells by drug inhibition of chromatin regulators did not lead to initiation of *ABCB1* expression. In addition to the altered chromatin modifications in the promoter region, we noted a clear detachment of the *ABCB1* locus from the NL in the Taxol-resistant cells. In

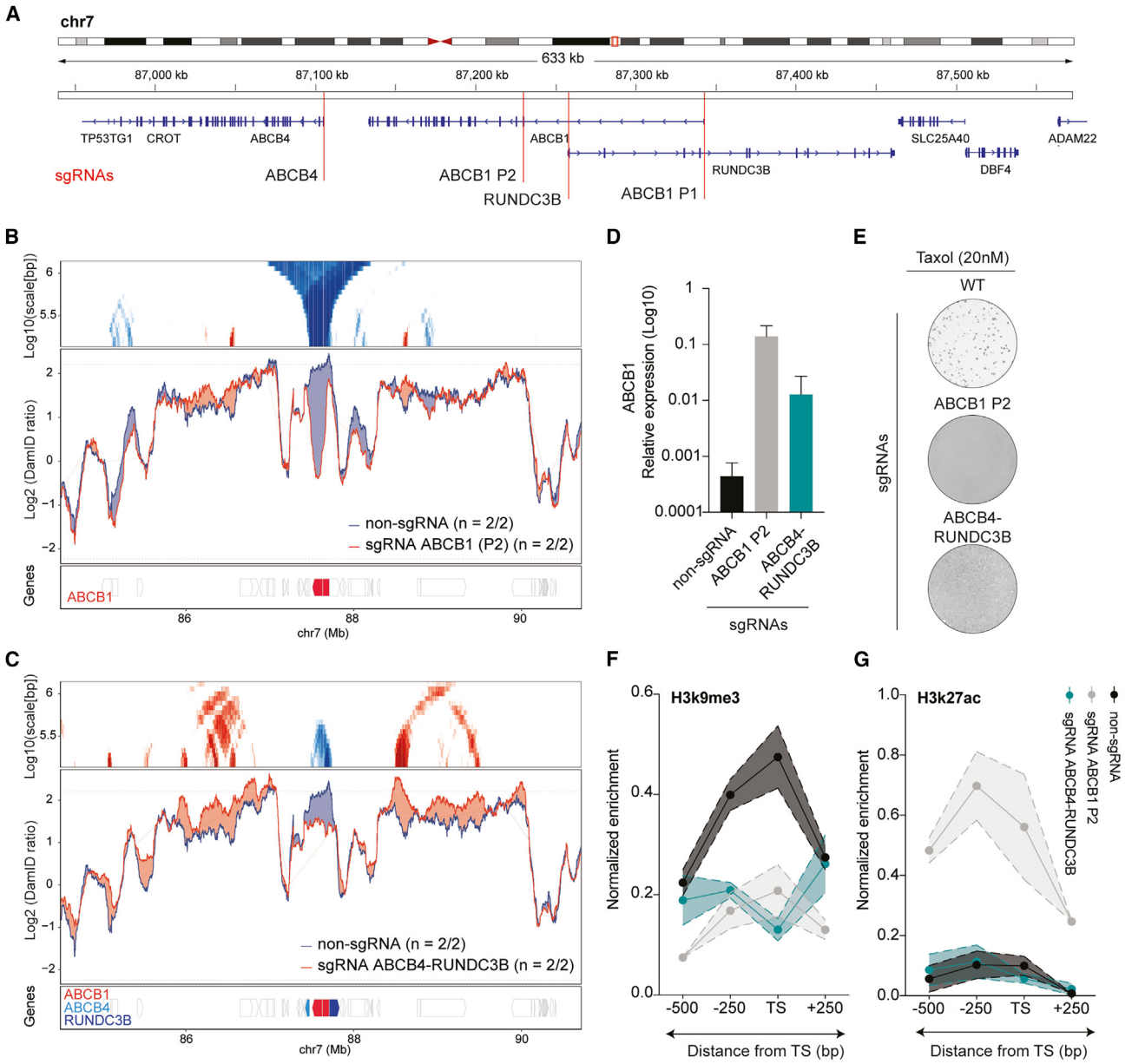

Figure 7. Transcription-driven CRISPRa activation of neighboring genes can detach *ABCB1* from the NL and lead to Taxol resistance

(A) Schematic representation of the Chr7q21.12 region indicating the locations where the sgRNAs were targeting for CRISPRa *ABCB1*, *ABCB4,* or *RUNDC3B* activation. Two regions were independently targeted to upregulate ABCB1: P1 (proximal promoter, 6 sgRNA were used) and P2 (internal promoter, a single sgRNA was used).

(B) Local NL detachment caused by CRISPRa *ABCB1* or (C) simultaneously CRISPRa *ABCB4* and *RUNDC3B* as analyzed in Figure 4A. Color key domainogram as in Figure 4A.

(D) *ABCB1* mRNA levels determined by qRT-PCR and normalized to *GAPDH* upon CRISPRa activation of *ABCB1* (P2) or combination of *ABCB4* and *RUNDC3B*. Error bas represent the SD of three independent experiments (n = 3).

(E) Crystal violet staining of viability assay on CRISPRa cell lines upon activation of *ABCB1* (P2) and the combination of *ABCB4* and *RUNDC3B*.

(F) ChIP-qPCR of H3K9me3 and (G) H3K27ac in the *ABCB1* regulatory region for CRISPRa WT, *ABCB1,* or the combination of *ABCB4* and *RUNDC3B* (B4-RUND). TS marks the transcription start site of the promoter. ChIP signal was normalized over input and a positive control specific for each mark. Area fill represents the SEM of six technical replicates coming from two independent experiments.

conjunction with that, disruption of the *LBR*, a key NL protein, led to enhanced acquisition of drug resistance, implying that NL detachment is a key step for *ABCB1* gene activation.

ABCB1 amplification and Taxol resistance

Complex genetic rearrangements have been observed in the *ABCB1* locus, which can also lead to acquired Taxol resistance.

Among them we can include gene amplifications and extra chromosomal DNA sequences containing the *ABCB1* gene.[60,61] By copy number analysis and microscopy, we detected a partial amplification of chromosome 7 in RPE-TxR cells, where *ABCB1* is located. It has been previously shown that upon chemotherapy treatment, chromosome 7 can be amplified leading to multidrug resistance.[11,60,62] Importantly, we show that a gain of chromosome 7 alone is not enough to acquire Taxol resistance in RPE-1 cells, as *ABCB1* remains transcriptionally repressed. We hypothesize that in order for RPE-1 cells to activate transcription of *ABCB1* (hence acquire Taxol resistance), a modification of its chromatin landscape is needed rather than accumulating increased copies of *ABCB1*.

Role of histone modifications and DNA methylation in the ABCB1 locus

ABCB1 gene regulation is thought to be driven by DNA methylation.[63] Some studies have shown that low DNA methylation status of the *ABCB1* promoter is linked to gene activation[15,16]; however, other studies were unable to confirm these findings.[17,18] Here we show that there is a switch from inactive to active chromatin in the *ABCB1* promoter in RPE-TxR cells. Nonetheless, we do not observe significant changes in DNA methylation pattern. Depletion of the DNA methyltransferase DNMT1 in RPE-TxS cells did not directly alter *ABCB1* gene expression or Taxol sensitivity. The same was observed when inhibiting the H3K27 methyltransferase EZH2, suggesting that the active chromatin environment observed in the *ABCB1* promoter region in RPE-TxR cells may be secondary to gene activation during the process of transcriptional derepression. In mammalian cells, disruption or inhibition of the H3K9me2 methyltransferase G9a has been shown to lead to weakened NL-LAD interactions[38,55,64,65]; however, our experiments show that G9a inhibition does not lead to *ABCB1* detachment from the NL or an increase in *ABCB1* gene expression. Interestingly, Bian et al. described that peripheral tethering of the HBB locus depends on both G9a-induced H3K9me2 and Suv39h1/2-induced H3K9me3 deposition.[64] This suggests that modifying a single histone chromatin mark may not be sufficient to trigger *ABCB1* detachment from the NL. Possibly, the change in chromatin features on the *ABCB1* gene are the consequence rather than cause of transcriptional activation.

How depletion of LBR may derepress ABCB1

Studies in *Drosophila* have found that depletion of lamins can lead to derepression of NL-associated genes.[39,66] Here, we found that *ABCB1* is partially activated upon depletion of *LBR* but not lamins. We speculate that depletion of *LBR* may lead to leaky *ABCB1* gene expression in at least two different ways. In one model, loss of *LBR* may cause stochastic detachment of *ABCB1* from the NL. In this respect it is important to note that our LBR KO cells are polyclonal, and that alterations in 3D genome organization may vary across the cells in the population. In mouse and human cells, *LBR* has been implicated in anchoring heterochromatin to the NL.[57,67,68] In our study, we observe that *ABCB1* contacts with the NL are not significantly altered after *LBR* depletion in general, but that *LBR* depletion can prime a subset of cells in our polyclonal population for activation of the *ABCB1* gene when exposed to Taxol. If stable contacts with the NL are essential for robust repression of *ABCB1*, then occasional detachment could account for the increased occurrence of Taxol-resistant clones in *LBR*-depleted cells. Indeed, NL interactions can be intrinsically stochastic, and the NL contact frequency is inversely linked to gene expression.[69,70] Notably, *LBR* has also been shown to catalyze a chemical reaction involved in cholesterol production.[71] Cholesterol is an important component of the nuclear membrane, which can directly affect nuclear integrity.[72] The fact that only a small proportion of cells acquire Taxol resistance could suggest that other mechanisms need to co-occur in order to fully activate *ABCB1*. In a second model, depletion of *LBR* may not only affect the *ABCB1*-NL contact frequency, but may also compromise the repressive potential of the NL. *LBR* may play a direct role in this repression, e.g., through its interaction with HP1,[73] or indirectly by controlling the protein composition of the NL. This partially defective repression in *LBR*-depleted cells could then allow for emergence of Taxol-resistant clones. It would be interesting to assess how exactly loss of *LBR* modifies the chromatin landscape within the *ABCB1* region. In fact, it has been shown that the N-terminal nucleoplasmic domain of *LBR* represses transcription and promotes condensation of chromatin.[74] In both models, interactions of *ABCB1* with the NL contribute to its repression.

Forced detachment of ABCB1 from the NL coincides with gene activation

The generation of CRISPRa cell lines targeting *ABCB4* and *RUNDC3B* allowed for detachment of *ABCB1* from the NL, and we find that this is associated with *ABCB1* gene activation. This further suggests a causal effect between NL detachment and *ABCB1* gene activation. However, we cannot fully rule out that the activated *ABCB4* and *RUNDC3B* promoters act as enhancers of the nearby *ABCB1* promoter, because enhancer activity has been observed for many promoters.[75] Also, we cannot rule out that transcriptional activation of neighboring genes can act as an initiator of *ABCB1* expression prior to NL detachment, which subsequently arises as a consequence of transcriptional activation. Interestingly, a decrease of gene expression has previously been observed by tethering chromosomes to the nuclear periphery.[76–78] Notably, recent research has shown that intrinsic features of promoters influence their sensitivity to the repressive LAD environment.[32] According to this study, the *ABCB1* promoter is classified as repressed in K562 cells and thereby to have the potential to be activated if taken out from its native repressive LAD environment.

Cell-type-specific roles of LBR and lamins

We find that depletion of *LBR*, but not Lamin A/C, or B, can render the *ABCB1* locus permissive to gene activation. In another study, Lamin A/C together with *LBR* were shown to be involved in tethering heterochromatin to the nuclear periphery during development.[57] Interestingly, a recent study shows that loss of Lamin B1 leads to detachment of LADs together with global chromatin re-distribution and de-compaction, supporting the idea that NL has a role in chromatin dynamics and potentially in gene regulation.[79] Our results show that only *LBR* depletion

has a positive effect on the induction of Taxol resistance in RPE-1 cells. This could be because in differentiated cells, NL components may have different relevance on lamina destabilization. Certainly, *LBR* may have cell-type-specific effects, as we observed with the depletion of *LBR* in the various cancer cell lines. Importantly, we did not observe *LBR* expression changes in RPE-TxR cells compared with RPE-TxS (Figure S6G). This suggests that altered *LBR* expression is not per se required for activation of a gene associated with the NL. Instead, it may be that *LBR* depletion destabilizes NL interactions. We speculate that other mechanisms could be occurring during promoter NL detachment in the RPE-TxR cells. The same could be speculated for A549 or other cells with high levels of both *ABCB1* and *LBR*.

Limitations of the study

While all our results are compatible with a model in which gene reactivation is primed by NL detachment of the locus containing that gene, our study does not definitively establish detachment of *ABCB1* from the NL as the first step in *ABCB1* gene derepression. The exact sequence of events leading to increased transcription remains unclear and might not always follow the same sequence of events. While CRISPRa experiments with *ABCB4* and *RUNDC3B* suggest that NL detachment could be the initial event in *ABCB1* activation, the potential influence of their transcription on the *ABCB1* promoter cannot be ruled out. Also, the effect of *LBR* loss on the acquisition of drug resistance varies across different cell lines, and the low frequency of drug-resistant colonies in some of the tested cell lines introduces a certain amount of uncertainty in quantitation. Finally, while our polyclonal *LBR* KO cell line displayed an increase in the frequency of drug-resistant colonies, we could not capture *ABCB1* transcription activation and NL detachment in the polyclonal *LBR* KO line, making it impossible to conclude that *LBR* loss is sufficient to detach the *ABCB1* locus from the NL. While it is possible that NL interaction of the *ABCB1* gene is lost in a subset of cells in this polyclonal population, we currently lack the evidence for this. To address this, single-cell RNA-sequencing and single-cell DamID will have to be employed in future studies, but given the low frequency of Taxol resistance, there are still several challenges to overcome to provide this level of evidence.

Taken together, we propose that acquisition of Taxol resistance in RPE-1 cells requires the *ABCB1* locus to loosen its interactions with the NL. This key step could be followed by changes in the local chromatin state that might help to keep the locus detached from the NL, altogether leading to *ABCB1* gene expression. Whether lamina detachment is a critical step in the derepression of an inactive gene likely depends on the contribution of lamina association in the regulation of gene expression of a given gene. One could envision that 3D genome rearrangements are an important priming step in the activation of a gene that is tightly associated to the NL, while activation of a TF is more likely to be the crucial event for activation of genes that display a more relaxed lamina association.

STAR★METHODS

Detailed methods are provided in the online version of this paper and include the following:

SUPPLEMENTAL INFORMATION

Supplemental information can be found online at https://doi.org/10.1016/j.celrep.2023.113124.

ACKNOWLEDGMENTS

We thank the NKI Genomics for excellent support, and members from our laboratories for inspiring and helpful discussions. This work was supported by NWO Zwaartekracht (58588) (to R.H.M.), by NIH Common Fund "4D Nucleome" Program grant U54DK107965 (to B.v.S.), and an MSCA IF (grant agreement 838555) and MSCA Young Researcher Fellowship (EU-MUR, Next Generation EU) (to S.G.M). The Oncode Institute is partly supported by the KWF Dutch Cancer Society.

AUTHOR CONTRIBUTIONS

Conceived and designed study: A.G.M., R.H.M., B.v.S. Experiments: A.G.M., S.G.M., S.P., L.P., D.P.H, A.F., M.I., S.J., H.T. Data processing, bioinformatics: T.S., N.Q.L., S.P., K.F., S.J., V.F.D.S, E.d.W., B.v.S. Discussion and interpretation of data: A.G.M., S.G.M., S.P., R.H.M., B.v.S. Manuscript writing: A.G.M., R.H.M., B.v.S., with input from all authors.

DECLARATION OF INTERESTS

E.d.W. is a co-founder of Cergentis B.V.

INCLUSION AND DIVERSITY

We support inclusive, diverse, and equitable conduct of research.

Received: February 18, 2021
Revised: August 5, 2023
Accepted: August 25, 2023

REFERENCES

1. Holohan, C., Van Schaeybroeck, S., Longley, D.B., and Johnston, P.G. (2013). Cancer drug resistance: An evolving paradigm. Nat. Rev. Cancer *13*, 714–726. https://doi.org/10.1038/nrc3599.
2. Rebucci, M., and Michiels, C. (2013). Molecular aspects of cancer cell resistance to chemotherapy. Biochem. Pharmacol. *85*, 1219–1226. https://doi.org/10.1016/j.bcp.2013.02.017.
3. Du, Z., and Lovly, C.M. (2018). Mechanisms of receptor tyrosine kinase activation in cancer. Mol. Cancer *17*, 58. https://doi.org/10.1186/s12943-018-0782-4.
4. Rosenzweig, S.A. (2018). Acquired Resistance to Drugs Targeting Tyrosine Kinases. In Advances in Cancer Research (Academic Press Inc.), pp. 71–98. https://doi.org/10.1016/bs.acr.2018.02.003.
5. General Mechanisms of Drug Resistance - Holland-Frei Cancer Medicine - NCBI Bookshelf https://www.ncbi.nlm.nih.gov/books/NBK12424/.
6. Jaenisch, R., and Bird, A. (2003). Epigenetic regulation of gene expression: How the genome integrates intrinsic and environmental signals. Nat. Genet. *33*, 245–254. https://doi.org/10.1038/ng1089.
7. Albertson, D.G. (2006). Gene amplification in cancer. Trends Genet. *22*, 447–455. https://doi.org/10.1016/j.tig.2006.06.007.
8. Dedes, K.J., Wilkerson, P.M., Wetterskog, D., Weigelt, B., Ashworth, A., and Reis-Filho, J.S. (2011). Synthetic lethality of PARP inhibition in cancers lacking *BRCA1* and *BRCA2* mutations. Cell Cycle *10*, 1192–1199. https://doi.org/10.4161/cc.10.8.15273.
9. Housman, G., Byler, S., Heerboth, S., Lapinska, K., Longacre, M., Snyder, N., and Sarkar, S. (2014). Drug resistance in cancer: An overview. Cancers *6*, 1769–1792. https://doi.org/10.3390/cancers6031769.
10. Goldstein, L.J. (1996). MDR1 gene expression in solid tumours. Eur. J. Cancer *32A*, 1039–1050. https://doi.org/10.1016/0959-8049(96)00100-1.
11. Vaidyanathan, A., Sawers, L., Gannon, A.L., Chakravarty, P., Scott, A.L., Bray, S.E., Ferguson, M.J., and Smith, G. (2016). ABCB1 (MDR1) induction defines a common resistance mechanism in paclitaxel- and olaparib-resistant ovarian cancer cells. Br. J. Cancer *115*, 431–441. https://doi.org/10.1038/bjc.2016.203.
12. Christie, E.L., Pattnaik, S., Beach, J., Copeland, A., Rashoo, N., Fereday, S., Hendley, J., Alsop, K., Brady, S.L., Lamb, G., et al. (2019). Multiple ABCB1 transcriptional fusions in drug resistant high-grade serous ovarian and breast cancer. Nat. Commun. *10*, 1295. https://doi.org/10.1038/s41467-019-09312-9.
13. Patch, A.M., Christie, E.L., Etemadmoghadam, D., Garsed, D.W., George, J., Fereday, S., Nones, K., Cowin, P., Alsop, K., Bailey, P.J., et al. (2015). Whole-genome characterization of chemoresistant ovarian cancer. Nature *521*, 489–494. https://doi.org/10.1038/nature14410.
14. Yasui, K., Mihara, S., Zhao, C., Okamoto, H., Saito-Ohara, F., Tomida, A., Funato, T., Yokomizo, A., Naito, S., Imoto, I., et al. (2004). Alteration in Copy Numbers of Genes as a Mechanism for Acquired Drug Resistance. Cancer Res. *64*, 1403–1410. https://doi.org/10.1158/0008-5472.CAN-3263-2.
15. Desiderato, L., Davey, M.W., and Piper, A.A. (1997). Demethylation of the human MDR1 5' region accompanies activation of P-glycoprotein expression in a HL60 multidrug resistant subline. Somat. Cell Mol. Genet. *23*, 391–400. https://doi.org/10.1007/bf02673749.
16. Chen, K.G., Wang, Y.C., Schaner, M.E., Francisco, B., Durán, G.E., Juric, D., Huff, L.M., Padilla-Nash, H., Ried, T., Fojo, T., and Sikic, B.I. (2005). Genetic and epigenetic modeling of the origins of multidrug-resistant cells in a human sarcoma cell line. Cancer Res. *65*, 9388–9397. https://doi.org/10.1158/0008-5472.CAN-04-4133.
17. Li, A., Song, J., Lai, Q., Liu, B., Wang, H., Xu, Y., Feng, X., Sun, X., and Du, Z. (2016). Hypermethylation of ATP-binding cassette B1 (ABCB1) multidrug resistance 1 (MDR1) is associated with cisplatin resistance in the A549 lung adenocarcinoma cell line. Int. J. Exp. Pathol. *97*, 412–421. https://doi.org/10.1111/iep.12212.
18. Reed, K., Hembruff, S.L., Laberge, M.L., Villeneuve, D.J., Côté, G.B., and Parissenti, A.M. (2008). Hypermethylation of the ABCB1 downstream gene promoter accompanies ABCB1 gene amplification and increased expression in docetaxel-resistant MCF-7 breast tumor cells. Epigenetics *3*, 270–280. https://doi.org/10.4161/epi.3.5.6868.
19. Kalmykova, A.I., Nurminsky, D.I., Ryzhov, D.V., and Shevelyov, Y.Y. (2005). Regulated chromatin domain comprising cluster of co-expressed genes in Drosophila melanogaster. Nucleic Acids Res. *33*, 1435–1444. https://doi.org/10.1093/nar/gki281.
20. Razin, S.V., Farrell, C.M., and Recillas-Targa, F. (2003). Genomic domains and regulatory elements operating at the domain level. Int. Rev. Cytol. *226*, 63–125. https://doi.org/10.1016/S0074-7696(03)01002-7.
21. Dillon, N. (2006). Gene regulation and large-scale chromatin organization in the nucleus. Chromosome Res. *14*, 117–126. https://doi.org/10.1007/s10577-006-1027-8.
22. Hansen, J.C. (2006). Linking genome structure and function through specific histone acetylation. ACS Chem. Biol. *1*, 69–72. https://doi.org/10.1021/cb6000894.
23. Sproul, D., Gilbert, N., and Bickmore, W.A. (2005). The role of chromatin structure in regulating the expression of clustered genes. Nat. Rev. Genet. *6*, 775–781. https://doi.org/10.1038/nrg1688.
24. Hildebrand, E.M., and Dekker, J. (2020). Mechanisms and Functions of Chromosome Compartmentalization. Trends Biochem. Sci. *45*, 385–396. https://doi.org/10.1016/J.TIBS.2020.01.002.
25. Razin, S.V., and Gavrilov, A.A. (2020). The Role of Liquid–Liquid Phase Separation in the Compartmentalization of Cell Nucleus and Spatial Genome Organization. Biochem *85*, 643–650. https://doi.org/10.1134/S0006297920060012.
26. Flavahan, W.A., Drier, Y., Liau, B.B., Gillespie, S.M., Venteicher, A.S., Stemmer-Rachamimov, A.O., Suvà, M.L., and Bernstein, B.E. (2016). Insulator dysfunction and oncogene activation in IDH mutant gliomas. Nature *529*, 110–114. https://doi.org/10.1038/nature16490.
27. Seaman, L., Chen, H., Brown, M., Wangsa, D., Patterson, G., Camps, J., Omenn, G.S., Ried, T., and Rajapakse, I. (2017). Nucleome analysis reveals structure-function relationships for colon cancer. Mol. Cancer Res. *15*, 821–830. https://doi.org/10.1158/1541-7786.MCR-16-0374.
28. Hnisz, D., Weintraub, A.S., Day, D.S., Valton, A.L., Bak, R.O., Li, C.H., Goldmann, J., Lajoie, B.R., Fan, Z.P., Sigova, A.A., et al. (2016). Activation of proto-oncogenes by disruption of chromosome neighborhoods. Science (80- *351*, 1454–1458. https://doi.org/10.1126/science.aad9024.
29. Martin, P., McGovern, A., Orozco, G., Duffus, K., Yarwood, A., Schoenfelder, S., Cooper, N.J., Barton, A., Wallace, C., Fraser, P., et al. (2015). Capture Hi-C reveals novel candidate genes and complex long-range interactions with related autoimmune risk loci. Nat. Commun. *6*, 10069. https://doi.org/10.1038/ncomms10069.
30. Lupiáñez, D.G., Kraft, K., Heinrich, V., Krawitz, P., Brancati, F., Klopocki, E., Horn, D., Kayserili, H., Opitz, J.M., Laxova, R., et al. (2015). Disruptions of topological chromatin domains cause pathogenic rewiring of gene-enhancer interactions. Cell *161*, 1012–1025. https://doi.org/10.1016/j.cell.2015.04.004.
31. Katainen, R., Dave, K., Pitkänen, E., Palin, K., Kivioja, T., Välimäki, N., Gylfe, A.E., Ristolainen, H., Hänninen, U.A., Cajuso, T., et al. (2015). CTCF/cohesin-binding sites are frequently mutated in cancer. Nat. Genet. *47*, 818–821. https://doi.org/10.1038/ng.3335.

32. Leemans, C., van der Zwalm, M.C.H., Brueckner, L., Comoglio, F., van Schaik, T., Pagie, L., van Arensbergen, J., and van Steensel, B. (2019). Promoter-Intrinsic and Local Chromatin Features Determine Gene Repression in LADs. Cell *177*, 852–864.e14. https://doi.org/10.1016/j.cell.2019.03.009.

33. Peric-Hupkes, D., Meuleman, W., Pagie, L., Bruggeman, S.W.M., Solovei, I., Brugman, W., Gräf, S., Flicek, P., Kerkhoven, R.M., van Lohuizen, M., et al. (2010). Molecular Maps of the Reorganization of Genome-Nuclear Lamina Interactions during Differentiation. Mol. Cell *38*, 603–613. https://doi.org/10.1016/j.molcel.2010.03.016.

34. Wen, B., Wu, H., Shinkai, Y., Irizarry, R.A., and Feinberg, A.P. (2009). Large histone H3 lysine 9 dimethylated chromatin blocks distinguish differentiated from embryonic stem cells. Nat. Genet. *41*, 246–250. https://doi.org/10.1038/ng.297.

35. Harr, J.C., Luperchio, T.R., Wong, X., Cohen, E., Wheelan, S.J., and Reddy, K.L. (2015). Directed targeting of chromatin to the nuclear lamina is mediated by chromatin state and A-type lamins. J. Cell Biol. *208*, 33–52. https://doi.org/10.1083/jcb.201405110.

36. Berman, B.P., Weisenberger, D.J., Aman, J.F., Hinoue, T., Ramjan, Z., Liu, Y., Noushmehr, H., Lange, C.P.E., Van Dijk, C.M., Tollenaar, R.A.E.M., et al. (2011). Regions of focal DNA hypermethylation and long-range hypomethylation in colorectal cancer coincide with nuclear laminag-associated domains. Nat. Genet. *44*, 40–46. https://doi.org/10.1038/ng.969.

37. van Steensel, B., and Belmont, A.S. (2017). Lamina-Associated Domains: Links with Chromosome Architecture, Heterochromatin, and Gene Repression. Cell *169*, 780–791. https://doi.org/10.1016/j.cell.2017.04.022.

38. Chen, H., Zheng, X., and Zheng, Y. (2014). Age-associated loss of lamin-b leads to systemic inflammation and gut hyperplasia. Cell *159*, 829–843. https://doi.org/10.1016/j.cell.2014.10.028.

39. Shevelyov, Y.Y., Lavrov, S.A., Mikhaylova, L.M., Nurminsky, I.D., Kulathinal, R.J., Egorova, K.S., Rozovsky, Y.M., and Nurminsky, D.I. (2009). The B-type lamin is required for somatic repression of testis-specific gene clusters. Proc. Natl. Acad. Sci. USA *106*, 3282–3287. https://doi.org/10.1073/pnas.0811933106.

40. Ito, K., Awano, W., Suzuki, K., Hiromi, Y., and Yamamoto, D. (1997). The Drosophila mushroom body is a quadruple structure of clonal units each of which contains a virtually identical set of neurones and glial cells. Development *124*, 761–771. 8223268.

41. Tame, M.A., Manjón, A.G., Belokhvostova, D., Raaijmakers, J.A., and Medema, R.H. (2017). TUBB3 overexpression has a negligible effect on the sensitivity to taxol in cultured cell lines. Oncotarget *8*, 71536–71547. https://doi.org/10.18632/oncotarget.17740.

42. Trcek, T., Lionnet, T., Shroff, H., and Lehmann, R. (2017). mRNA quantification using single-molecule FISH in Drosophila embryos. Nat. Protoc. *12*, 1326–1348. https://doi.org/10.1038/nprot.2017.030.

43. Huff, L.M., Lee, J.S., Robey, R.W., and Fojo, T. (2006). Characterization of gene rearrangements leading to activation of MDR-1. J. Biol. Chem. *281*, 36501–36509. https://doi.org/10.1074/jbc.M602998200.

44. Fojo, T. (2007). Multiple paths to a drug resistance phenotype: Mutations, translocations, deletions and amplification of coding genes or promoter regions, epigenetic changes and microRNAs. Drug Resist. Updates *10*, 59–67. https://doi.org/10.1016/j.drup.2007.02.002.

45. Robinson, J.T., Turner, D., Durand, N.C., Thorvaldsdóttir, H., Mesirov, J.P., and Aiden, E.L. (2018). Juicebox.js Provides a Cloud-Based Visualization System for Hi-C Data. Cell Syst. *6*, 256–258.e1. https://doi.org/10.1016/J.CELS.2018.01.001.

46. Wang, X.Q.D., and Dostie, J. (2017). Chromosome folding and its regulation in health and disease. Curr. Opin. Genet. Dev. *43*, 23–30. https://doi.org/10.1016/j.gde.2016.10.006.

47. de Vree, P.J.P., de Wit, E., Yilmaz, M., van de Heijning, M., Klous, P., Verstegen, M.J.A.M., Wan, Y., Teunissen, H., Krijger, P.H.L., Geeven, G., et al. (2014). Targeted sequencing by proximity ligation for comprehensive variant detection and local haplotyping. Nat. Biotechnol. *32*, 1019–1025. https://doi.org/10.1038/nbt.2959.

48. Huang, C., and Zhu, B. (2018). Roles of H3K36-specific histone methyltransferases in transcription: antagonizing silencing and safeguarding transcription fidelity. Biophys. Rep. *4*, 170–177. https://doi.org/10.1007/s41048-018-0063-1.

49. Nicetto, D., and Zaret, K.S. (2019). Role of H3K9me3 heterochromatin in cell identity establishment and maintenance. Curr. Opin. Genet. Dev. *55*, 1–10. https://doi.org/10.1016/J.GDE.2019.04.013.

50. Heintzman, N.D., Stuart, R.K., Hon, G., Fu, Y., Ching, C.W., Hawkins, R.D., Barrera, L.O., Van Calcar, S., Qu, C., Ching, K.A., et al. (2007). Distinct and predictive chromatin signatures of transcriptional promoters and enhancers in the human genome. Nat. Genet. *39*, 311–318. https://doi.org/10.1038/ng1966.

51. van Schaik, T., Vos, M., Peric-Hupkes, D., HN Celie, P., and van Steensel, B. (2020). Cell cycle dynamics of lamina-associated DNA. EMBO Rep. *21*, e50636. https://doi.org/10.15252/embr.202050636.

52. Brueckner, L., Zhao, P.A., van Schaik, T., Leemans, C., Sima, J., Peric-Hupkes, D., Gilbert, D.M., and van Steensel, B. (2020). Local rewiring of genome–nuclear lamina interactions by transcription. EMBO J.685255 https://doi.org/10.1101/685255.

53. Germier, T., Kocanova, S., Walther, N., Bancaud, A., Shaban, H.A., Sellou, H., Politi, A.Z., Ellenberg, J., Gallardo, F., and Bystricky, K. (2017). Real-Time Imaging of a Single Gene Reveals Transcription-Initiated Local Confinement. Biophys. J. *113*, 1383–1394. https://doi.org/10.1016/j.bpj.2017.08.014.

54. Yokochi, T., Poduch, K., Ryba, T., Lu, J., Hiratani, I., Tachibana, M., Shinkai, Y., and Gilbert, D.M. (2009). G9a selectively represses a class of late-replicating genes at the nuclear periphery. Proc. Natl. Acad. Sci. USA *106*, 19363–19368. https://doi.org/10.1073/PNAS.0906142106.

55. Kind, J., Pagie, L., Ortabozkoyun, H., Boyle, S., De Vries, S.S., Janssen, H., Amendola, M., Nolen, L.D., Bickmore, W.A., and Van Steensel, B. (2013). Single-cell dynamics of genome-nuclear lamina interactions. Cell *153*, 178–192. https://doi.org/10.1016/j.cell.2013.02.028.

56. van den Berg, J., G Manjón, A., Kielbassa, K., Feringa, F.M., Freire, R., and Medema, R.H. (2018). A limited number of double-strand DNA breaks is sufficient to delay cell cycle progression. Nucleic Acids Res. *46*, 10132–10144. https://doi.org/10.1093/nar/gky786.

57. Solovei, I., Wang, A.S., Thanisch, K., Schmidt, C.S., Krebs, S., Zwerger, M., Cohen, T.V., Devys, D., Foisner, R., Peichl, L., et al. (2013). LBR and lamin A/C sequentially tether peripheral heterochromatin and inversely regulate differentiation. Cell *152*, 584–598. https://doi.org/10.1016/j.cell.2013.01.009.

58. Wong, X., Hoskins, V.E., Melendez-Perez, A.J., Harr, J.C., Gordon, M., and Reddy, K.L. (2021). Lamin C is required to establish genome organization after mitosis. Genome Biol. *22*, 305–327. https://doi.org/10.1186/S13059-021-02516-7/FIGURES/7.

59. Rullens, P.M.J., and Kind, J. (2021). Attach and stretch: Emerging roles for genome–lamina contacts in shaping the 3D genome. Curr. Opin. Cell Biol. *70*, 51–57. https://doi.org/10.1016/J.CEB.2020.11.006.

60. Genovese, I., Ilari, A., Assaraf, Y.G., Fazi, F., and Colotti, G. (2017). Not only P-glycoprotein: Amplification of the ABCB1-containing chromosome region 7q21 confers multidrug resistance upon cancer cells by coordinated overexpression of an assortment of resistance-related proteins. Drug Resist. Updates *32*, 23–46. https://doi.org/10.1016/j.drup.2017.10.003.

61. Ruiz, J.C., Choi, K.H., von Hoff, D.D., Roninson, I.B., and Wahl, G.M. (1989). Autonomously replicating episomes contain mdr1 genes in a multidrug-resistant human cell line. Mol. Cell Biol. *9*, 109–115. https://doi.org/10.1128/mcb.9.1.109.

62. Ibrahim, S.M., Karim, S., Abusamra, H., Pushparaj, P.N., Khan, J.A., Abuzenadah, A.M., Gari, M.A., Bakhashab, S., Ahmed, F., and Al-Qahtani, M.H. (2018). Genomic amplification of chromosome 7 in the Doxorubicin

resistant K562 cell line. Bioinformation *14*, 587–593. https://doi.org/10.6026/97320630014587.

63. Zappe, K., and Cichna-Markl, M. (2020). Aberrant DNA Methylation of ABC Transporters in Cancer. Cells *9*. https://doi.org/10.3390/cells9102281.
64. Bian, Q., Khanna, N., Alvikas, J., and Belmont, A.S. (2013). β-Globin cis-elements determine differential nuclear targeting through epigenetic modifications. J. Cell Biol. *203*, 767–783. https://doi.org/10.1083/JCB.201305027.
65. Li, Z., Jiao, X., Di Sante, G., Ertel, A., Casimiro, M.C., Wang, M., Katiyar, S., Ju, X., Klopfenstein, D.V., Tozeren, A., et al. (2019). Cyclin D1 integrates G9a-mediated histone methylation. Oncogene *3822*, 4232–4249. https://doi.org/10.1038/s41388-019-0723-8.
66. Ulianov, S.V., Doronin, S.A., Khrameeva, E.E., Kos, P.I., Luzhin, A.V., Starikov, S.S., Galitsyna, A.A., Nenasheva, V.V., Ilyin, A.A., Flyamer, I.M., et al. (2019). Nuclear lamina integrity is required for proper spatial organization of chromatin in Drosophila. Nat. Commun. *10*, 1176. https://doi.org/10.1038/s41467-019-09185-y.
67. Poleshko, A., Mansfield, K.M., Burlingame, C.C., Andrake, M.D., Shah, N.R., and Katz, R.A. (2013). The Human Protein PRR14 Tethers Heterochromatin to the Nuclear Lamina during Interphase and Mitotic Exit. Cell Rep. *5*, 292–301. https://doi.org/10.1016/j.celrep.2013.09.024.
68. Clowney, E.J., Legros, M.A., Mosley, C.P., Clowney, F.G., Markenskoff-Papadimitriou, E.C., Myllys, M., Barnea, G., Larabell, C.A., and Lomvardas, S. (2012). Nuclear aggregation of olfactory receptor genes governs their monogenic expression. Cell *151*, 724–737. https://doi.org/10.1016/j.cell.2012.09.043.
69. Kind, J., Pagie, L., de Vries, S.S., Nahidiazar, L., Dey, S.S., Bienko, M., Zhan, Y., Lajoie, B., de Graaf, C.A., Amendola, M., et al. (2015). Genome-wide maps of nuclear lamina interactions in single human cells. Cell *163*, 134–147. https://doi.org/10.1016/j.cell.2015.08.040.
70. Rooijers, K., Markodimitraki, C.M., Rang, F.J., de Vries, S.S., Chialastri, A., de Luca, K.L., Mooijman, D., Dey, S.S., and Kind, J. (2019). Simultaneous quantification of protein-DNA contacts and transcriptomes in single cells. Nat. Biotechnol. *37*, 766–772. https://doi.org/10.1038/s41587-019-0150-y.
71. Tsai, P.L., Zhao, C., Turner, E., and Schlieker, C. (2016). The Lamin B receptor is essential for cholesterol synthesis and perturbed by disease-causing mutations. Elife *5*, e16011. https://doi.org/10.7554/ELIFE.16011.
72. Ramjiawan, B., Czubryt, M.P., Gilchrist, J.S., Pierce, G.N., and Biology, O. (1996). Nuclear Membrane Cholesterol Can Modulate Nuclear Nucleoside Tri phosphatase Activity. J. Cell. Biochem. *63*, 442–452.
73. Polioudaki, H., Kourmouli, N., Drosou, V., Bakou, A., Theodoropoulos, P.A., Singh, P.B., Giannakouros, T., and Georgatos, S.D. (2001). Histones H3/H4 form a tight complex with the inner nuclear membrane protein LBR and heterochromatin protein 1. EMBO Rep. *2*, 920–925. https://doi.org/10.1093/embo-reports/kve199.
74. Hirano, Y., Hizume, K., Kimura, H., Takeyasu, K., Haraguchi, T., and Hiraoka, Y. (2012). Lamin B receptor recognizes specific modifications of histone H4 in heterochromatin formation. J. Biol. Chem. *287*, 42654–42663. https://doi.org/10.1074/jbc.M112.397950.
75. Medina-Rivera, A., Santiago-Algarra, D., Puthier, D., and Spicuglia, S. (2018). Widespread Enhancer Activity from Core Promoters. Trends Biochem. Sci. *43*, 452–468. https://doi.org/10.1016/j.tibs.2018.03.004.
76. Finlan, L.E., Sproul, D., Thomson, I., Boyle, S., Kerr, E., Perry, P., Ylstra, B., Chubb, J.R., and Bickmore, W.A. (2008). Recruitment to the nuclear periphery can alter expression of genes in human cells. PLoS Genet. *4*, e1000039. https://doi.org/10.1371/journal.pgen.1000039.
77. Reddy, K.L., Zullo, J.M., Bertolino, E., and Singh, H. (2008). Transcriptional repression mediated by repositioning of genes to the nuclear lamina. Nature *452*, 243–247. https://doi.org/10.1038/nature06727.
78. Dialynas, G., Speese, S., Budnik, V., Geyer, P.K., and Wallrath, L.L. (2010). The role of Drosophila Lamin C in muscle function and gene expression. Development *137*, 3067–3077. https://doi.org/10.1242/dev.048231.
79. Chang, L., Li, M., Shao, S., Li, C., Ai, S., Xue, B., Hou, Y., Zhang, Y., Li, R., Fan, X., et al. (2022). Nuclear peripheral chromatin-lamin B1 interaction is required for global integrity of chromatin architecture and dynamics in human cells. Protein Cell *13*, 258–280. https://doi.org/10.1007/s13238-020-00794-8.
80. Friskes, A., Koob, L., Krenning, L., Severson, T.M., Koeleman, E.S., Vergara, X., Schubert, M., van den Berg, J., Evers, B., Manjón, A.G., et al. (2022). Double-strand break toxicity is chromatin context independent. Nucleic Acids Res. *50*, 9930–9947. https://doi.org/10.1093/NAR/GKAC758.
81. Sanjana, N.E., Shalem, O., and Zhang, F. (2014). Improved vectors and genome-wide libraries for CRISPR screening. Nat. Methods *11*, 783–784. https://doi.org/10.1038/NMETH.3047.
82. Shalem, O., Sanjana, N.E., Hartenian, E., Shi, X., Scott, D.A., Mikkelson, T., Heckl, D., Ebert, B.L., Root, D.E., Doench, J.G., and Zhang, F. (2014). Genome-scale CRISPR-Cas9 knockout screening in human cells. Science *343*, 84–87. https://doi.org/10.1126/SCIENCE.1247005.
83. Jacobi, A.M., Rettig, G.R., Turk, R., Collingwood, M.A., Zeiner, S.A., Quadros, R.M., Harms, D.W., Bonthuis, P.J., Gregg, C., Ohtsuka, M., et al. (2017). Simplified CRISPR tools for efficient genome editing and streamlined protocols for their delivery into mammalian cells and mouse zygotes. Methods *121–122*, 16–28. https://doi.org/10.1016/j.ymeth.2017.03.021.
84. Prekovic, S., Schuurman, K., Mayayo-Peralta, I., Manjón, A.G., Buijs, M., Yavuz, S., Wellenstein, M.D., Barrera, A., Monkhorst, K., Huber, A., et al. (2021). Glucocorticoid receptor triggers a reversible drug-tolerant dormancy state with acquired therapeutic vulnerabilities in lung cancer. Nat. Commun. *121*, 4360. https://doi.org/10.1038/s41467-021-24537-3.
85. Durinck, S., Moreau, Y., Kasprzyk, A., Davis, S., De Moor, B., Brazma, A., and Huber, W. (2005). BioMart and Bioconductor: A powerful link between biological databases and microarray data analysis. Bioinformatics *21*, 3439–3440. https://doi.org/10.1093/bioinformatics/bti525.
86. van Heeringen, S.J., and Veenstra, G.J.C. (2011). GimmeMotifs: A de novo motif prediction pipeline for ChIP-sequencing experiments. Bioinformatics *27*, 270–271. https://doi.org/10.1093/bioinformatics/btq636.
87. Liu, N.Q., Maresca, M., van den Brand, T., Braccioli, L., Schijns, M.M.G.A., Teunissen, H., Bruneau, B.G., Nora, E. èP., and de Wit, E. (2020). WAPL maintains a cohesin loading cycle to preserve cell-type-specific distal gene regulation. Nat. Genet. *531.53*, 100–109. https://doi.org/10.1038/s41588-020-00744-4.

STAR★METHODS

KEY RESOURCES TABLE

REAGENT or RESOURCE	SOURCE	IDENTIFIER
Antibodies		
H3k27me3	Actif Motif	Cat# #39155; RRID:AB_2561020
H3k9me2	Abcam	Cat# ab1220; RRID:AB_449854
Lamin B1	Abcam	Cat# ab16048; RRID:AB_443298
Goat anti-rabbit Alexa Fluor 488-conjugated secondary antibody	Invitrogen; Thermo Fisher Scientific	Cat# A11008; RRID:AB_143165
Goat anti-mouse Alexa Fluor 568-conjugated secondary antibody	Invitrogen; Thermo Fisher Scientific	Cat# A11004; RRID:AB_253407
SMC1	Bethyl	Cat# A300-055A; RRID:AB_2192467
Alpha-tubulin	Sigma-Aldrich	Cat# T5168; RRID:AB_477579
DNMT1	Sigma-Aldrich	Cat# D4692; RRID:AB_262096
H3k27ac	Actif Motif	Cat# 39133; AB_2722569
Lamin A/C	Santa Cruz	Cat# sc6215; RRID:AB_648152
Lamin B Receptor (LBR)	Abcam	Cat# ab122919; RRID:AB_10902156
Polyclonal Goat Anti-Rabbit Immunoglobulins/HRP	Dako	Cat# P448; RRID:AB_2617138
Polyclonal Goat Anti-Mouse Immunoglobulins/HRP	Dako	Cat# P447; RRID:AB_2617137
Polyclonal Rabbit Anti-Goat Immunoglobulins/HRP	Dako	Cat# P449; RRID:AB_2617143
H3k9me3	Abcam	Cat# ab8898; RRID:AB_306848
H2AZ	Abcam	Cat# ab4174; RRID:AB_30434
H3k4me1	Abcam	Cat# ab8895; RRID:AB_306847
H3k4me3	Abcam	Cat# ab8580; RRID:AB_306649
H3k36me3	Abcam	Cat# ab9050; RRID:AB_306966
Lamin B2	Abcam	Cat# ab8983; RRID:AB_306912
Chemicals, peptides, and recombinant proteins		
Dimethyl sulfoxide (DMSO)	Sigma-Aldrich	Cat# D8418
DMEM/F-12	Gibco	Cat# 11320033
RPMI 1640	Gibco	Cat#: 21875034
DMEM	Gibco	Cat# 11965092
Fetal Bovine Serum	Serana	Cat# S-FBS-EU-015
Penicillin-Streptomycin	Gibco	Cat# 15070063
Sodium Piruvate	Gibco	Cat# 11360070

(*Continued on next page*)

Continued

REAGENT or RESOURCE	SOURCE	IDENTIFIER
HEPES	Gibco	Cat# 15630080
Prolong Gold Antifade Mountant	Invitrogen; Thermo Fisher Scientific	Cat# P36934
Lipofectamine RNAiMAX	Thermo Fisher Scientific	Cat# 13778150
M3814 (DNAPKi)	Selleckchem	Cat# S8586
Gibson Assembly® Master Mix	Biolabs	Cat# E2611S
Taxol (Paclitaxel)	Sigma-Aldrich	Cat# 33069-62-4
5-Aza-2-deoxycytidine	Sigma-Aldrich	Cat# A3656
GSK126	Selleckchem	Cat# S7061
BIX-01294	Selleckchem	Cat# S8006
NEB 5x Taq master mix	Biolabs	Cat# M0285L
Phusion® High-Fidelity DNA Polymerase	Biolabs	Cat# M0530S
SSC Buffer 20x Concentrate	Sigma-Aldrich	Cat# S6639
Formamide (Deionized)	Thermo Fisher Scientific	Cat# AM9342
Fugene 6	Promega	Cat# E5911
Dynabeads™ Protein A	Thermo Fisher Scientific	Cat# 10001D
SuperScript™ II Reverse Transcriptase	Thermo Fisher Scientific	Cat# 18064014
Critical commercial assays		
RNeasy Mini Kit	Qiagen	Cat# 74104
BioScript™ Reverse Transcriptase	Bioline	Cat# BIO-27036
PowerUp SYBR Green Master Mix	Thermo Fisher Scientific	Cat# A25742
QIAquick Gel Extraction Kit	Qiagen	Cat# 28704
Dual-Luciferase® Reporter Assay System Kit	Promega	Cat# E1910
ISOLATE II Genomic DNA Kit	Meridian Bioscience	Cat #BIO-52067
EpiJET Bisulfite Conversion Kit	Thermo Fisher Scientific	Cat# K1461
MyTaq Red HS Mix	Meridian Bioscience	Cat# BIO-25046
Experimental models: Cell lines		
RPE-hTERT iCut	van den Berg et al.[56]	N/A
RPE-hTERT CRISPRa	Brueckner et al.[52]	N/A
A549	NKI Cryostorage	N/A
MDA-MB-231	NKI Cryostorage	N/A
FADU	NKI Cryostorage	N/A
Oligonucleotides		
sgRNAs for CRISPRa, see Table S1	This paper	N/A
crRNAs for RPE iCUT KOs, see Table S2	This paper	N/A
RT-qPCR and ChIP-qPCR primers, see Table S3	This paper	N/A
RT-qPCR primers position, see Table S4	This paper	N/A
Recombinant DNA		
ANCHOR3 plasmids	NeoVirTech	N/A
pUC19 plasmid	Addgene	Cat# 49793
pSpCas9(BB)-2A-Puro (PX459)	Addgene	Cat# 62988
pSpCas9(BB)-2A-Puro-ABCB1	This paper	N/A
pGL3-Basic Vector GenBank®	Addgene	GenBank: U47295
pGL3-Promoter Vector GenBank®	Addgene	GeneBank: U47298
pRL-SV40 Vector GenBank®	Addgene	GeneBank: AF025845
pGL3-ABCB1	This paper	N/A

(*Continued on next page*)

Continued

REAGENT or RESOURCE	SOURCE	IDENTIFIER
Software and algorithms		
Adobe Photoshop	Adobe	RRID: SCR_014199; https://www.adobe.com/au/products/photoshop.html
Adobe Illustrator	Adobe	RRID: SCR_010279; https://www.adobe.com/au/products/illustrator.html
Microsoft 365	Microsoft	https://www.microsoft.com/en-au/microsoft-365/microsoft-office
GraphPad Prism 9.3.1	GraphPad	RRID: SCR_002798; https://www.graphpad.com/
Burrows-Wheeler Aligner (BWA) 0.5.9	SciCrunch Registry	RRID:SCR_010910; https://bio-bwa.sourceforge.net/
MACS3 software	SciCrunch Registry	RRID:SCR_013291; https://github.com/macs3-project/MACS
Deseq2	SciCrunch Registry	RRID:SCR_015687; https://bioconductor.org/packages/release/bioc/html/DESeq2.html
TopHat 2.1.1	SciCrunch Registry	RRID:SCR_013035; http://ccb.jhu.edu/software/tophat/index.shtml
IMARIS	SciCrunch Registry	RRID:SCR_007370; http://www.bitplane.com/imaris/imaris
Bismark 0.23.0	SciCrunch Registry	RRID:SCR_005604; http://www.bioinformatics.babraham.ac.uk/projects/bismark/
BioMaRt package	SciCrunch Registry	RRID:SCR_019214; https://bioconductor.org/packages/biomaRt/
GimmeMotifs	SciCrunch Registry	RRID:SCR_001146; http://131.174.198.125/bioinfo/gimmemotifs/
Cis-bp database 3.0	SciCrunch Registry	RRID:SCR_017236; http://cisbp.ccbr.utoronto.ca
Deposited data		
GEO accession code	This paper	GSE163315
GEO accession code, ChIPseq RPE TxS cells	Friskes et al.[80]	GSE210402
Other		
Code to align and process pA-DamID samples from Novaseq	GitHub (Bas van Steensel)	https://github.com/vansteensellab/pADamID_ABCB1_Novaseq
Code to process pA-DamID dominograms and correlation plots	GitHub (Bas van Steensel)	https://github.com/vansteensellab/domainograms/tree/manjon_etal

RESOURCE AVAILABILITY

Lead contact

Further information and requests for resources and reagents should be directed to and will be fulfilled by the lead contact, Rene H Medema (r.medema@nki.nl).

Materials availability

Cell lines used in this study contains the ANCHOR3 system that has been licensed from NeoVirTech (France). Cell line recipients will need to have an MTA from NeoVirTech.

Data and code availability

- RNA-seq, ChIP-seq, TLA and pA-DamID data have been deposited at GEO and are publicly available as of the date of publication. Accession numbers are listed in the key resources table. All data reported in this paper will be shared by the lead contact upon request.
- This paper reports original code for pA-DamID analysis, has been deposited at GitHub and is publicly available as of the date of publication. Links to them are listed in the key resources table.
- Any additional information required to reanalyze the data reported in this paper is available from the lead contact upon request.

METHOD DETAILS

Cell lines and cell culture conditions

hTert-immortalized retinal pigment epithelium (RPE-1) and derived cell lines were maintained in DMEM/F-12 + Glutamax (Gibco, Life Technology) supplemented with 1% penicillin/streptomycin and 6% fetal bovine serum (FBS, S-FBS-EU-015, Serana). RPE-1 iCUT (Cas9) cells to generate the KOs were obtained from.[56] A549 cancer cell lines were grown in Advanced RPMI 1640 (Gibco, Life Technology) supplemented with 1% penicillin/streptomycin, 1% sodium pyruvate, 2% HEPES buffer and 10% fetal bovine serum. MDA-MB-231 and FADU cell lines were maintained in DMEM (Gibco, Life Technology) supplemented with 1% penicillin/streptomycin, 1% sodium pyruvate, 2% HEPES buffer and 10% fetal bovine serum. All cell lines were routinely checked for mycoplasma.

RPE-1 ANCHOR3 cell lines generations

RPE-1 ANCHOR3 cells were generated from RPE-1 iCUT (Cas9) cells.[56] Three independent Phusion PCRs were done in order to amplify first the ANCH3 sequence from pANCH3 (NeoVirTech, France), second the homology right arm from the integration point downstream the ABCB1 locus (250bp).

Primers:5′GAATTCGAGCTCGGTACCAGAAGAGAAAGAAGAGCATTTATCAGGGG3′, 5′GCCGAGCTTGGCACCATA GCAGGAC AATAGGCAATGTT3’. And third, homology left arm from the integration point downstream the ABCB1 locus (250bp).

Primers:5′GCCTGCAGGTCGACTCTAGATTTGCGTTTGTTCATCAATAGAAGAAGGG3′, 5′CCTGCCAAAGTGACGCGAGGTCTAT AATTATTGGCATCTGATTTCATG3’.

PCR products were run in 2% agarose gel and purified with a gel extraction kit. ANCH3 sequence with *ABCB1* homology arms was cloned in a pUC19 plasmid with XbaI and KpnI restriction enzymes with a Gibson mix. sgRNA targeting *ABCB1* (CCTATT GTCCTGCTATGGCG) was cloned in a px459 following the manufacture protocol.[81] RPE-1 iCUT cells were nucleofected with 1ug of px459-sgRNA-ABCB1 and 2ug of pUC19-ANCH3 with M3814 (DNAPKi) to boost HDR-repair. Single clones were assessed for ANCH3 integration by PCR (see Sup. Figure S3A). Clone 9 was picked for following experiments. pLenti-eGFP-OR3-GFP (NeoVirTech, France), was transduced in Clone 9 followed by FACS sorting of GFP positive cells. From this population (ANCHOR3-OR3 GFP polyclonal) LBR and LMNA KOs were generated as well as drug treatments were performed. ANCHOR3-OR3-GFP cells were also treated with DMSO or Taxol to generate the ANCHOR3 TxS or TxR cells.

Drug treatments

Drugs were dissolved in DMSO and prepared at stock concentrations before usage at varying final concentrations as indicated in each figure. For the 24h assay, cells were treated for 24h with the specific epigenetic drug dose, adding 20nM of Taxol overnight followed by a wash out of the drugs and subsequently addition of 20nM Taxol again for 15 days. For the epigenetic drug treatment combination (Combo), 250nM of 5-Aza-2′-deoxycytidine (DNMT1i), 150nM of GSK126 (EZH2i) and 2uM of BIX-01294 (G9ai) were used.

Luciferase assay

The *ABCB1* promoter was cloned in a pGL3-basic (Promega) vector (pGL3-Basic Vector GenBank Accession Number U47295). The *ABCB1* internal promoter region (1kb) was PCR amplified from RPE-1 genomic DNA and inserted downstream of the luciferase reporter gene. The primers used were: gatcAAGCTTCATTAGCCAAATGCATGAGC (FWD) and GATCGGTACCTGGAAACAT CCTCAGACTATGC (REV). pGL3-promoter (Promega) vector (pGL3-Promoter Vector GenBank Accession Number U47298) was used as a control to assess transfection efficiency. For transfection of the pGL3 vectors, 2 million RPE-1 cells (TxS, TxR.3 or TxR.4) were resuspended in nucleofection buffer (Solution I and II 4:1). Solution I (125 mM Na2HPO4, 12.5 mM KCl, pH 7.75) Solution II (55 mM MgCl2). After co-transfection of 100ng of Renilla plasmid (pRL-SV40 Vector GenBank Accession Number AF025845) and 1 μg pGL3-basic-empty, 1 μg pGL3-basic-*ABCB1* or 1ug pGL3-promoter plasmid, cells were electroporated in an Amaxa 2D Nucleofector using program U-023. Cells were plated in 6-well plates and next day medium was changed. Luciferase reporter assay was performed 48h after nucleofection using a Dual-Luciferase Reporter assay kit (Promega). Cells were lysed directly on the plate with passive lysis buffer for 15 min at room temperature. Luciferase and Renilla activity were measured with the substrates from the kit using TECAN Infinite M200 PRO machine.

Generation of CRISPRa cell lines

For RPE-1 CRISPRa, sgRNAs targeting human *ABCB1* P1, *ABCB1* P2, *ABCB4*, *RUNDC3B*, intronic regions and *POU3F2*, *LHX6* and *ZIC5* were individually cloned into the lentiCRISPR v2 plasmid. Specific sequences are found on Sup. Table S1. CRISPR vectors were co-expressed with 3rd generation viral vectors in HEK293T cells using Fugene6 Transfection Reagent. After lentivirus production, the medium was harvested and transferred to the designated cell lines. Two days post infection cells were put on puromycin selection for two weeks.

tracrRNA:crRNA design and transfections in RPE-1 iCut

Alt-R crRNA (Integrated DNA technologies) for LBR, LMNB1 and LMNA were obtained from the Human CRISPR Knockout Pooled Library (GeCKO v2).[82] Specific sequences are found on Sup. Table S2 tracrRNA:crRNA duplex was transfected according to the manufacturer's protocol83.

RNA isolation and qRT-PCR analysis

RNA isolation was performed by using Qiagen RNeasy kit and quantified using NanoDrop (Thermo Fisher Scientific). cDNA was synthesized using Bioscript reverse transcriptase (Bioline), Random Primers (Thermo Fisher), and 1000 ng of total RNA according to the manufacturer's protocol. Primers were designed with a melting temperature close to 60° to generate 90–120-bp amplicons, mostly spanning introns. cDNA was amplified for 40 cycles on a cycler (model CFX96; Bio-Rad Laboratories) using SYBR Green PCR Master Mix (Applied Biosystems). Target cDNA levels were analyzed by the comparative cycle (Ct) method and values were normalized against GAPDH expression levels. qRT-PCR oligo sequences and positions are summarized in Sup. Tables S3 and S4, respectively.

siRNA transfections

ON-TARGETplus SMARTpool set of 4 siRNAs targeting LBR, POU3F2, LHX6 or ZIC5 were from Dharmacon and were transfected using RNAiMAX (Life Technologies) according to manufacturer's protocol[83] at a final concentration of 20nM. All transfections were performed 48h before experiment, if not specified on the figure legend. siRNA sequences can be found on Sup. Table S5.

Density and colony formation assays

1 million cells were treated indicated dose of Taxol and allowed to grow out for 15 days. Plates were fixed in 80% Methanol and stained with 0.2% Crystal Violet solution. Cell density was measured in ImageJ and normalized to control (WT) plate. For colony formation assays, the number of Taxol-resistant cells were counted.

Viability assays

For viability assays, 1000 cells were plated in a 96-well plate and treated for 7 days with indicated drug concentrations. Subsequently, plates were fixed in 80% Methanol and stained with 0.2% Crystal Violet solution.

Immunofluorescence

Cells were fixed with 3.7% formaldehyde and permeabilized with 0.2% Triton X-100 for 10 min. After, cells were blocked in 4% bovine serum albumin (BSA) in PBS supplemented with 0.1% Tween (PBS-T) for 1h. Cells were incubated for 2h at 4°C with primary antibody in PBS-T with 3% BSA, washed three times with PBS-T, and incubated with secondary antibody and DAPI in PBS-T with 3% BSA for 1h at room temperature (RT). Images were acquired with the use of a DeltaVision Elite (Applied Precision) equipped with a 60x 1.45 numerical aperture (NA) lens (Olympus) and cooled CoolSnap CCD camera. Nuclear intensity of the different chromatin marks was evaluated in ImageJ using an in-hose developed macro that enables automatic and objective analysis. The following antibodies were used for immunofluorescence experiments: H3K27me3 (Actif Motif #39155, 1:500), and H3K9me2 (ab1220, 1:500), Lamin B1 (ab16048, 1:500). Secondary antibodies were anti-rabbit Alexa 488 (A11008 Molecular probes, 1:600), anti-mouse Alexa 568 (A11004 Molecular probes, 1:600). DAPI was used at a final concentration of 1 μg/mL.

Western blots

For Western blot experiments, equal amounts of cells were lysed with Laemmli buffer and separated by SDS–polyacrylamide gel electrophoresis followed by transfer to a nitrocellulose membrane. Membranes were blocked in 5% milk in PBST for 1h at RT before overnight incubation with primary antibody in PBST with 3% BSA at 4°C. Membranes were washed three times with PBST followed by incubation with secondary antibody in PBST with 5% milk for 2h at RT. Antibodies were visualized using enhanced chemiluminescence (ECL) (GE Healthcare). The following antibodies were used for Western blot experiments: SMC1 (Bethyl, A300-055a), a-Tubulin (Sigma t5168), DNMT1 (Sigma, D4692), H3K27me3 (Actif Motif #39156), H3K27ac (Actif Motif #39133), H3K9me2 (ab1220), LaminB1 (ab16048), LaminA (sc6215) and Lamin B Receptor (ab232731). For secondary antibodies, peroxidase-conjugated goat anti-rabbit (P448 DAKO, 1:2000), goat anti-mouse (P447 DAKO, 1:2000) and rabbit anti-goat (P449) were used.

RNA FISH

RPE-1 cells were plated on glass coverslips and washed twice with BS before fixation in 4% PFA in PBS for 10 min at room temperature. After two additional washes in 1x PBS coverslips were incubated in 70% ethanol at 4°C overnight. Coverslips were incubated

for pre-hybridization in wash buffer (2x saline sodium citrate (SSC) with deionized formamide (Sigma) 10%) for 2–5 min at room temperature. RNA FISH probe mix wash dissolved in hybridization buffer (wash buffer supplemented with 10% dextran sulfate). 38 probes labeled with Cy5 were targeted to the intronic regions of ABCB1 (Biosearch technologies). Coverslips were incubated in hybridization solution for at least 4h at 37°C. Then coverslips were washed twice for 30 min with wash buffer followed by a quick rinse with 2x SSC. Finally, coverslips were washed once for 5 min in 1x PBS before mounting on slides using Prolong gold DAPI mounting medium (Life Technologies). Images were acquired with the use of a DeltaVision Elite (Applied Precision) equipped with a 60x 1.45 numerical aperture (NA) lens (Olympus) and cooled CoolSnap CCD camera. ABCB1 transcription start site quantification was performed manually double blind.

Quantification of the number of taxol-resistant colonies in siLBR treated cells

As a proliferation disadvantage was somehow observed when depleting *LBR* by RNA interference, we decided to quantify the number of Taxol resistant colonies relative to siLBR. We therefore calculated the siLBR effect by dividing the number of siLBR/siNT cells in the non-Taxol clonogenic assays (Sup. Figure S7C). We next divided the number of Taxol resistant colonies in Sup. Figure S7D by the siLBR effect. In the the non-Taxol clonogenic assays 100 cells were plated. In the clonogenic assays with Taxol 1 million cells were plated.

ChIP-sequencing and ChIP-qPCRs of RPE-1 hTERT cells

Chromatin immunoprecipitations (ChIP) were performed as described previously[84] with minor adjustments. Antibodies (5 μg) targeting specific histone modifications (H3K27ac, Actif Motif #39133; H3K9me3, ab8898; H2AZ, ab4174; H3K4me1, abcam 8895; H3K4me3, abcam 8580; and H3K36me3, abcam 9050) were bound to Protein A magnetic beads (Invitrogen) a day before the ChIP procedure. ChIP samples were then processed using a KAPA Biosystems kit for library preparation, sequenced on an Illumina Hiseq2500 genome analyzer (with 65bp reads, single end), and aligned to the human reference genome (hg19) using the Burrows-Wheeler Aligner (bwa) version 0.5.9. The mapped reads were filtered based on mapping quality (with a threshold of 20) using samtools version 0.1.19. The MACS3 software was used with default parameters for peak calling. Genome browser tracks were generated using EaSeq (http://easeq.net).

For ChIP-qPCR analysis, the DNA was amplified for 40 cycles using SYBR Green PCR Master Mix (Applied Biosystems) on a cycler (model CFX96; Bio-Rad Laboratories). The target DNA levels were analyzed by the comparative cycle (Ct) method and values were normalized against input DNA and positive control regions specific for each histone modification. The locations of the ChIP-qPCR oligos are summarized in Table S3.

RNA-sequencing

Total RNA from cultured cells was extracted using RLT (Qiagen). Strand-specific libraries were generated using the TruSeq PolyA Stranded mRNA sample preparation kit (Illumina). In brief, polyadenylated RNA was purified using oligo-dT beads. Following purification, the RNA was fragmented, random-primed and reserve transcribed using Sup.erScript II Reverse Transcriptase (Invitrogen). The generated cDNA was 3′ end-adenylated and ligated to Illumina Paired-end sequencing adapters and amplified by PCR using HiSeq SR Cluster Kit v4 cBot (Illumina). Libraries were analyzed on a 2100 Bioanalyzer (Agilent) and subsequently sequenced on a HiSeq2000 (Illumina). We performed RNAseq alignment using TopHat 2.1.1. Differentially expressed genes were called with DEseq2, with an adjusted p value threshold of 0.05.

Image analysis in 3D

Immunofluorescent images of RPE-1 ANCHOR3 with Lamin B1 staining were acquired with an LSM 980 Airyscan 2 on Zeiss Axio Observer 7 SP inverted microscope. Distance measurements in 3D were carried out in IMARIS (Oxford Instruments). The nuclear lamina was segmented using thresholding and smoothing options of the surface creation wizard. The ANCHOR3-dots were detected as spots of 0.8 μm size and filtered on maximum intensity. All ANCHOR3-segmentations were manually reviewed and edited if necessary. Once established for an experiment, the surface and spots creation wizards were run in batch. From the segmented images, the parameter of shortest distance to spots at the ANCHOR3-locus were exported.

Bisulfite treatment and analysis

Bisulfite sequencing was performed with RPE-1 cells TxS (RPE-0), TxR (RPE-10 and RPE-20) and RPE-1 treated with DMSO, DNMT1i (62.5nM) or G9ai (2uM) for 72h. gDNA extraction was performed with ISOLATE II Genomic DNA Kit (BIO-52067). Bisulfite conversion-PCR was done by converting 500ng of genomic DNA with the EpiJET Bisulfite Conversion Kit #K1461 according to product manual. Targeted amplification of the two CpG islands in the *ABCB1* promoter was achieved by using 3ul of converted DNA as PCR template using Standard MyTaq HS Mix (BIO-25046). Used primer sequences: *ABCB1* prom1 (GTTGATTGGTTGG GTAGGAATAG and AAACTATCCCATAATAACTCCCAACTT); *ABCB1* prom2 (TGGTAAGTTTATGGGGATTAAG and TAAACACTAC AAAAACTTTCCTAT). After purification amplified regions were used as template for a second round of PCR with indexed primers using NEB 5x Taq master mix (M0285L). Libraries were sequenced on a MiSeq nano with 250pb paired-end reads. Reads were aligned to Hg19 and methylation percentages were determined using Bismak version 0.23.0.

TLA analysis

TLA was performed as previously described with minor modifications.[47] TLA libraries were sequenced on a MiSeq and were analyzed with a custom TLA mapping pipeline. TLA ligation data were mapped to hg19. Normalization and downstream analysis were done using peakC16.

pA-DamID and sequencing

pA-DamID was performed as described previously with minor modifications.[51] We used a 1:200 dilution for Lamin B2 (Abcam ab8983, mouse) and a 1:500 dilution was used for Lamin B1 (Abcam ab16048, rabbit). pA-DamID library preparation was also performed as previously described.[51] However, during the performance of some of the experiments for this manuscript the NKI genomic and sequencing facility performed a transition from HiSeq to Novaseq Illumina platform. This required an adaptation of the pA-DamID protocol to dual-color Illumina technology. Here we report the pA-DamID library preparation for Novaseq. After pA-DamID and genomic DNA extraction 500 ng of genomic DNA were digested with 10 U of DpnI in CutSmart Buffer 1X, for 8 h at 37°C, followed by heat inactivation at 80°C for 20 min. To 10 μl of Digestion mix 5 μl A-tailing mix (0.5 μL of Cutsmart buffer 10X, 0.25 μL Klenow 50 U/uL, 0.05 μL dATP 100 mM, 4.2 μL H2O) were added. A-tailing was performed at 37° for 30′, followed by heat inactivation for 20′ at 75°C. Adapter ligation was performed by adding to the A-tailed mix 15 μL of adapter ligation mix (3 μL T4 Roche Ligase Buffer 10X, 0.5 μL T4 ligase (5 U/uL), 0,25 μl of x-Gene Stubby Adapter 50 μM (IDT),11.25 μl H2O) and incubated 16 h at 16°, followed by heat inactivation at 65° for 10 min. Methyl Indexed PCR was performed by amplifying 4uL of ligated DNA with x-Gen Dual combinatorial Indexes (IDT) at 125 nM final concentration, using MyTaq RedMix (Bioline) and the following PCR program: 1 X (1′ 94°C), 15 X (30″ 94°C, 30″ 58°C, 30″ 72°C), 1X (2′ 72°C). Correlations between pA-DamID replicates can be found on Sup. Table S6. The bioinformatic pipeline to align and process pA-DamID samples from Novaseq sequencing can be found here: https://github.com/vansteensellab/pADamID_ABCB1_Novaseq

Visualization and measurement of gene detachment from the nuclear lamina

To visualize detachment of genes from the nuclear lamina we used a domainogram function as previously described.[52] For the gene correlation plots, the pA-DamID score was calculated using GATC read counts. This is the sum of all GATC counts calculated over the gene length +/− 10 kb calculated both for Dam-only and Lmnb2 samples. Gene scores then undergo to three types of normalization:1) Library size by normalizing Dam and Lmnb2 samples for 1M of reads with a normalization factor. 2) Dam/Lmnb2 log2 ratio. 3) *Z* score normalization to minimize variability across experiments and obtain similar dynamic ranges.

Motif analysis

Genomic coordinates of all the genes were obtained from GRCh37 (Ensembl version 75) using biomaRt package[85] and transcription starting sites of the genes were extend 1 kb to both up- and down-stream to identify the promoter regions. The motifs presenting in the promoters were identified using GimmeMotifs[86] against the non-redundant *Cis*-bp database (version 3.0). To identify the over-represented motifs, we used a similar method as described in.[87] Briefly, we calculated for every motif the frequency in the promoters of the upregulated genes and all the expressed genes. We computed relative motif frequency by dividing the individual motif frequency by to total number of identified motifs. We calculated the log2-enrichment score by calculating the ratio of relative motif frequency between the promoters of up-regulated genes and all the expressed genes. The p value was calculated using the Fisher exact test on the following 2x2 table: for every motif M, we determine the number of the promoters belonging to the upregulated genes with or without M and for the promoters of the expressed genes with or without M.

QUANTIFICATION AND STATISTICAL ANALYSIS

Except for pA-DamID, statistical analysis was performed using GraphPad Prism v9.3.1. pA-DamID experiments were processed and analyzed in R with Rstudio, the figures were generated using ggplot2. The main packages and software are listed in the key resource table and information about statistical analysis is available in the scripts (github). Statistical methods, number of replicates (n), and error bars are described in figure legends and method details. Figures were prepared using Adobe Photoshop and Illustrator.